The Impact of Improved Surface Boundary Conditions on Titan's Climate Patterns

Colin Baciocco

Juan Lora and Mark Brandon

May 12, 2021

A Senior Thesis presented to the faculty of the Department of Earth and Planetary Sciences, Yale University, in partial fulfillment of the Bachelor's Degree.

Abstract

To better model and assess Titan's regional climates with general circulation models (GCMs), GCMs must incorporate the characteristics of each of Titan's geomorphological terrains. Accordingly, we created GCM-readable maps of three different parameters important to the circulation of an atmosphere over a surface – roughness lengths, albedos, and topography – by either modifying previously-published maps or using an analogue-based procedure. We included some of these maps in the Titan Atmospheric Model (TAM), an intermediate-complexity Titan GCM. We hypothesized that adding heterogenous surface properties to TAM would cause simulated surface temperatures to better fit those observed in the thermal emissions analysis of Jennings et al. (2019). We also hypothesized that including spatially heterogeneous roughness lengths to the GCM would modify wind speeds, especially in the polar regions and over the northern polar lakes, which may have wind-driven surface waves [Hayes et al., 2016]. We calculated skill scores for surface temperatures in the model and found that heterogeneous roughness lengths helped the model to better fit surface temperature observations when compared to a control; however, adding both heterogeneous roughness lengths and atmospherically-relevant topography to TAM made the fit worse. When examining the modeled surface winds over Titan's three seas, we found that the addition of roughness lengths or topography induced some variation in the mean wind (on the order of 0.1 to 0.3 m/s) relative to the control. There were larger variations from the control evident in the daily maximum wind (e.g. increases in maximum wind speeds of up to 50%). The addition of topography, or albedo and topography, also caused the mean wind to increase such that it was then sufficient to create wind-driven surface waves over some seas as determined by the wind speed thresholds of Hayes et al. (2013).

1 Introduction

Various techniques have been used to model Titan's atmosphere and climate [Pollack, 1973; Lora et al., 2015]. One technique is the general circulation model (GCM), which has been useful for constraining discussions of Titan's climate given the relatve sparseness of data on the subject when compared to Earth. A number of Titan GCMs have been created [Lora et al., 2019]. Those which have been developed or substantially updated within the last decade include the Institut Pierre Simon Laplace GCM (hereafter the IPSL model), the University of Cologne (Köln) GCM (hereafter the Köln model), the Titan Weather, Research, and Forecasting Model (hereafter "TitanWRF"), and the Titan Atmospheric Model (TAM) [Lora et al., 2019; Newman et al., 2016]. These and past GCMs have been used to examine a number of phenomena in Titan's atmosphere. Such phenomena includes Titan's atmospheric superrotation, methane cycle, paleoclimates, and interactions between the surface and atmosphere [Tokano, 2005; Lora et al., 2015, Faulk et al., 2017; Lora et al., 2014; Tokano, 2019].

Recent model intercomparisons have shown that Titan's general atmosphere and surface environment now seem fairly well-constrained. Observations and models show slow low-level winds (almost always below 5 m s^{-1} in all directions) and atmospheric temperatures which vary by about 2 K [Lora et al., 2019]. Given the in-situ measurements provided by the Huygens probe, atmospheric profiles about the equator are particularly well-constrained. However, some models fit these profiles better than others. TAM and TitanWRF fit the observed zonal wind profile much better than the IPSL and Köln models, and TAM additionally provides good fits to the methane mole fraction and temperature profiles, something TitanWRF does not perform [Lora et al., 2019; Newman et al., 2016]. Diurnal and seasonal variations are less well-constrained and more model dependent, but general diurnal variation seems to be about 1-1.5 K according to models and observations, and seasonal variation seems to be about 1-3 K according to the Köln model [Cottini et al., 2010; Tokano, 2019; Lora et al., 2019]. These general diurnal variations may be misleading for certain regions, however, as the general estimates of 1-1.5 K were based on estimates of surface thermal inertia being 300–600 TIU ($J \cdot m^{-2} \cdot K^{-1} \cdot s^{-\frac{3}{2}}$) [Mackenzie et al., 2019]. These thermal inertia estimates may be true for the majority of Titan's surface, but they could underestimate the thermal inertia of Titan's lakes by a factor of about 30 if those lakes are deeply convective [Mackenzie et al., 2019]. This could then lead to additional thermal damping in diurnal and even seasonal variations in some of the regions where lakes are present, like the northern pole. Estimates of the methane cycle are even less comparable from model to model, as almost every model parameterizes methane cycle processes in significantly different ways,

but there is general agreement on the cycle's importance and large-scale influence. One example of this influence would be the way evaporative cooling is likely the primary reason for northern polar temperatures varying by a relatively small amount from season to season [Tokano, 2019].

Beyond solely modeling Titan's atmosphere, GCMs have also been used in studies of the evolution of Titan's climate and hydrology, or to evaluate the relative importance of forcings like the variations in its topography or orbital parameters. This has been attempted by coupling GCMs to other models of Titan systems, like the evolution of its Croll–Milankovitch cycle or its possible surface and subsurface "hydrology" [Tokano, 2005; Tokano, 2019; Faulk et al., 2020]. Some of this has already been productive in constraining possible surface types [Tokano, 2005]. Another paper, which examined the coupling of Titan's Croll-Milankovitch cycle, climate, and surface illustrated the relative importance of Titan's topography for its long-term (millenial) climate dynamics [Tokano, 2019].

These studies, which combine atmospheric models of Titan with other information on Titan systems, are also an example of the next frontier in studying Titan's climate: regional studies incorporating detailed information on Titan's surface generated from the full set of Cassini data products [Lora et al., 2019]. Some questions on Titan's meteorological or climatological phenomena can only be answered by improving the assumptions Titan GCMs make about the surface, such as by introducing spatial heterogeneities into the models' surface boundary conditions.

Accordingly, one question we posed for this study is, "does a TAM configuration with more information on Titan's surface better match observations of Titan's climate?" We hypothesized that adding heterogenous surface properties to TAM would cause simulated surface temperatures to better fit those observed in the thermal emissions analysis of Jennings et al. (2019). (This hypothesis does of course require that the heterogeneities added be somewhat realistic in location and degree.)

Another, slightly more complicated area of study which might benefit from the introduction of spatial heterogeneities into Titan GCMs' boundary conditions is the discussion of low-level surface winds over Titan's hydrocarbon seas, and whether those winds are high enough to generate waves of significant height (> 0.75 m). Waves > 0.75 m may be significant not just for their height but because they could be sufficient to cause shoreline erosion and help shape coastal morphologies [Hayes et al., 2016]. Wind-driven waves could also play a role in deepening the mixed layer of Titan's methane seas and lakes, and thus raise their bulk inertia by significant amounts, e.g. up to an order of magnitude or more [Hayes et al.,

2016; Mackenzie et al., 2019]. Assessing the possibilities for these waves' relative prevalence was thus another goal of this study. We additionally hypothesized that including spatially heterogeneous roughness lengths in TAM would modify wind speeds, especially over the northern polar seas, which may have wind-driven surface waves [Hayes et al., 2016].

2 Methods

To better model and assess Titan's regional climates with GCMs, models likely need to incorporate the characteristics of each of Titan's geomorphological terrains. This is because differences in the climates between different regions often arise from differences in the atmospherically-relevant properties of a surface, such as when moisture from bodies of water allows air parcels to rise beyond what would be permitted by the dry adiabatic lapse rate. Accordingly, we created GCM-readable maps of three different parameters important to the circulation of an atmosphere over a surface – roughness lengths for momentum, topography, and albedos – by either modifying previously-published data sets or by using an analogue-based procedure of inference and extrapolation which will be described in the following pages. We included some of these maps in TAM both individually and in two combinations. TAM models Titan's winds and near-surface climate well, as has been described, and also incorporates an active hydrological cycle. This hydrological cycle includes the on and below surface transport of methane, which could be an important factor in Titan's near-surface climate [Faulk et al., 2020]. We performed various assessments of regional surface temperatures and surface wind speeds, as well as the ways different model configurations affected these quantities.

As the goal of this thesis was to examine the possible influence of surface heterogeneties on Titan's atmosphere and climate, when given a choice between what a possible overestimate and a possible underestimate of surface heterogeneity, we tried to err towards overestimation. We did this in order to try and constrain the possible effects of surface heterogeneities.

2.1 Map Creation

The procedures we used to create the maps are as follows:

1. *Geomorphological Terrain:* The global terrain classifications and mapping of Lopes et al. (2019) are a very important part of the process of creating the maps of albedo and surface roughness lengths. To make the maps easily manipulable for use in a climate

model, however, we had to rasterize the shapefiles in which the terrain classifications were originally stored. To deal with the fact that the crater terrain of Lopes et al. (2019) can present a range of different surface types depending on crater age, we overwrote the classifications of the crater cells with the terrain classifications in Mackenzie et al. (2019), which does not use a crater unit but otherwise has the same terrain types as Lopes et al. (2019).

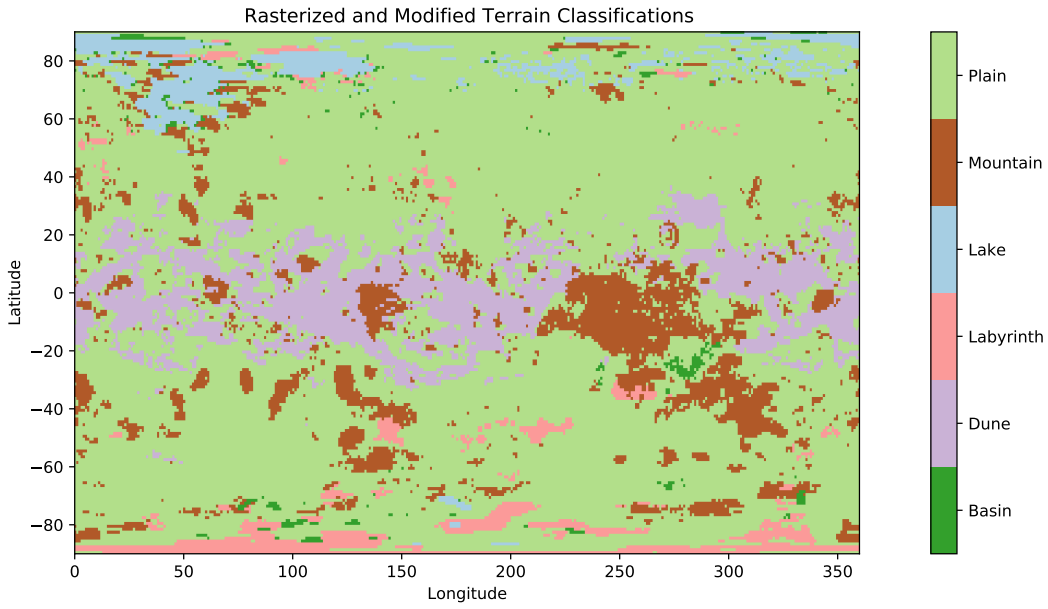

Figure 1: Geomorphological Terrain types according to Lopes et al. (2019), with Specified Modifications

2. *Albedo:* We based our estimates of global albedo patterns off two sources: our modified global map of geomorphological regions of Lopes et al. (2019), and the exploration of the regional albedo spectra and possible surface compositions of Solomonidou et al. (2018). TAM's radiative transfer model handles solar-wavelength (<4.5 µm) and thermal infrared (>4.5 µm) separately, so we produced two final maps: one for visible wavelength albedos, and one for albedos in the thermal infrared. For the visible wavelength albedos, we computed the albedos for each terrain in the terrain map using weighted averages of all Solomonidou et al. (2018)'s regional albedo values below 4.5 µm. (The weight function came from a spectrum of solar energy at any particular wavelength: Gueymard (2004). We decided not to weight by a spectrum of solar radiation at the bottom of the atmosphere because the necessity of using Titan radiative

transfer models to obtain the spectrum meant that such a weighting would introduce an additional and significant layer of assumptions.) We then assigned these average albedo values to their respective terrains in a rasterized version of the Lopes et al. (2019) map. To create the map of thermal wavelength albedos, we used Kirchoff's law and a map of emissivities from Janssen et al. (2016).

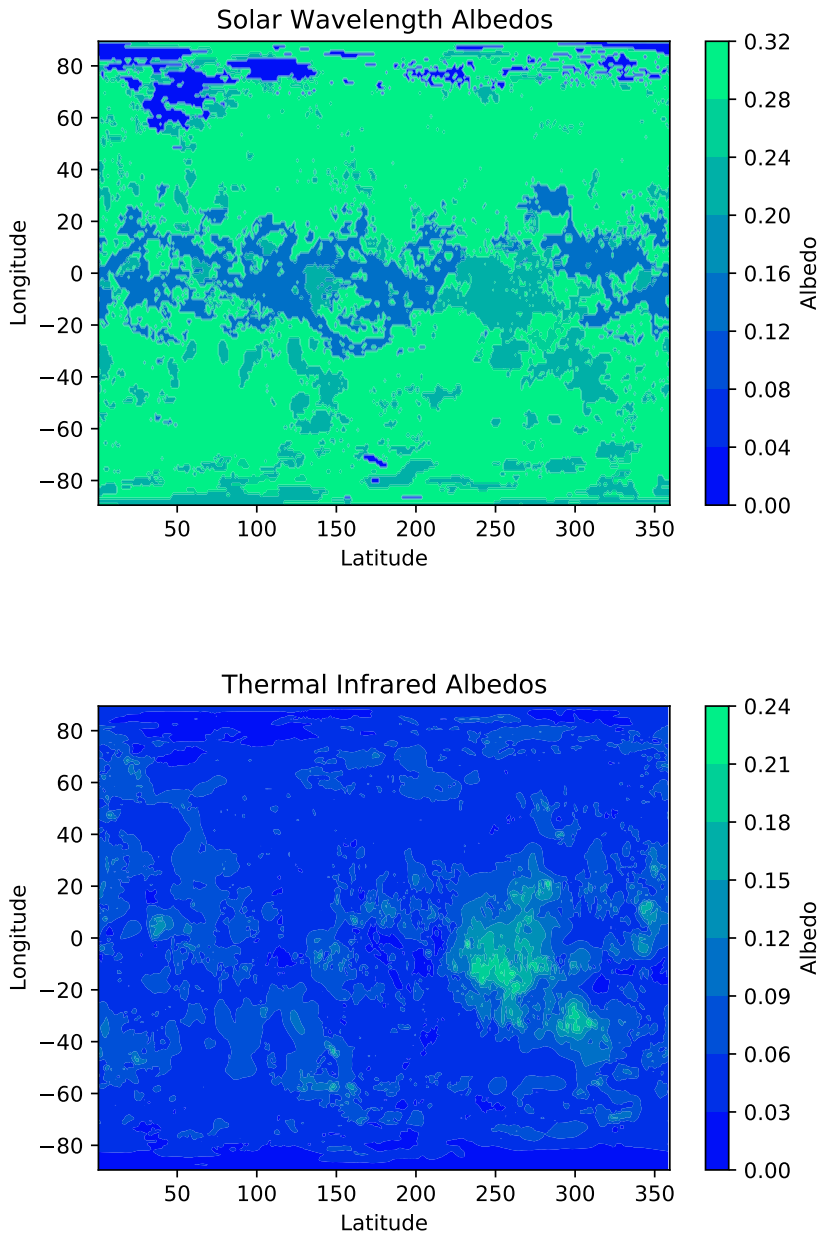

Figure 2: Solar-Wavelength and Thermal Infrared Albedos

3. *Roughness Lengths:* Similar to the albedo maps, we produced our map of roughness lengths by estimating plausible roughness lengths (for momentum) for each of the regions in the global geomorphological map of Lopes et al. (2019). Similarly to the solar-wavelength albedo map, each roughness length value was then assigned to its respective terrains on the rasterized version of the Lopes et al. (2019) map. Because the only published assessment of roughness lengths on Titan has come from images transmitted by Huygens, and is thus extremely limited in its spatial scale, we decided to use an approach based on analogies between largely unvegetated Earth environments – whose roughness lengths are comparatively well-described – and environments on Titan, which are mostly known by SAR (Synthetic Aperture Radar) observations at various resolutions. Roughness lengths are defined as a near-surface level of no motion in the logarithmic profile of near-surface wind speeds, which is itself a product of the boundary layer turbulence theory first put forward by Obukhov in 1946 [Heavens, 2008]. The logarithmic profile of near-surface wind speed is one of the most common techniques for modeling near-surface winds, and has the following form:

$$u_z = \frac{u_*}{\kappa}\left[\ln\left(\frac{z-d}{z_0}\right) + \psi\left(z, z_0, L\right)\right] \tag{1}$$

where u_* is the friction velocity, κ is the Von Kármán constant, d is the zero plane displacement, z_0 is the surface roughness length, and ϕ is a term which accounts for stability. In ϕ, L is the Obukhov length in Monin-Obukhov similarity theory. (Monin-Obukhov similarity theory is a method for describing non-dimensionalized mean flows and temperatures that is widely used in boundary-layer meteorology [Foken, 2006].) Note that if the atmosphere is neutrally stable, $\phi = 0$. Roughness lengths are an intrinsic characteristic of the surface, and depend on the surface's geometry and composition, not the local gravitational field or atmosphere.

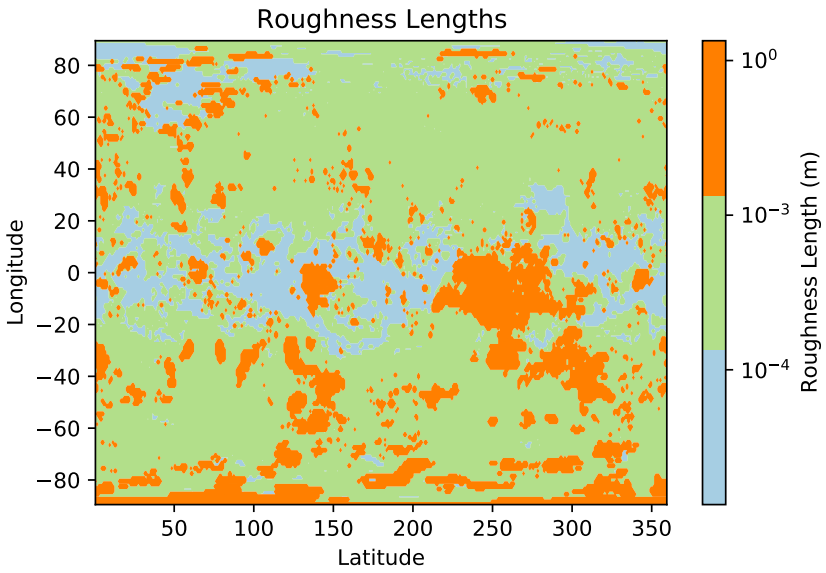

Figure 3: Roughness Lengths

Titan Terrain Type	**Earth Analog Assigned**	**Roughness Length (m)**	**Final Roughness Length (m)**	**Reference**
Plains	Between Flat Snow Field and Flat Rafted Ice	0.0007-0.003	0.001	Hansen, 1993 (flat desert); Wiernga, 1993 (flat rafted ice)
Dunes	Sand Dunes (Namib Desert)	0.0002	0.0001	Prijent et al., 2005
Hummocky	Mountain Range (At most lightly vegetated)	1.7	1	Rejimer et al., 2003
Lakes / Seas	Calm Open Sea	0.0001	0.0001	Hansen, 1993
Labyrinth	Forested Ridges, 150 m to 200 m	3	1	Hansen, 1993

Table 1: Roughness Length Values and Titan Terrain Analogues for Roughness Lengths

The rationale behind these classifications was the following:

- *Plains:* Though far from homogeneous, this was the terrain where the Huygens probe landed and, compared to Titan's other terrains, it is relatively well-studied. Images from the landing site have allowed surface roughness to be calculated as roughly 5×10^{-3} m [Tokano, 2006].
- *Dunes:* We classified Titan's dunes as being analogous to the size, shape, and arrangement of the large dunes (a.k.a. "ergs") in the Namib Desert following the Titan community's overwhelming consensus that such an analogy was appropriate [Lopes, et al., 2019].

- *Hummocky:* We classified the hummocky terrains as being analogous to unvegetated, roughly 2-km-high mountain ranges on Earth. Lopes et al. (2019) describes their paper's hummocky terrain as consisting of "mountain chains and isolated terrains that are topographically higher than the surrounding areas." These chains are "a few to tens of kilometers in length and up to a couple of kilometres high above the reference geoid" [Lopes et al, 2019]. We researched roughness lengths for regions of lightly-vegetated or unvegetated Earth mountain ranges of comparable height, and found that 1.7 meters was a widely-agreed-upon value for roughness lengths on the mountains of that size [Lancaster, 2004; Technical University of Denmark, 2019]. Not all of the land areas included in a mountain chain may have roughness lengths as high as 1.7 m, but any overestimation of roughness lengths is still likely to help us to establish an upper bound for the possible effects of surface heterogeneity.
- *Lakes/Seas:* We classified the lakes/seas as being analogous to flat lakes and seas on Earth. We did this because Cassini observed "remarkably calm" lake and sea surfaces during most of its mission, which lasted from the middle of Titan's northern hemisphere winter to the northern hemisphere's summer solstice (Hayes, 2016). It has been hypothesized that low-level winds would pick up later in the mission, as Titan moved later into the northern hemisphere's summer, and cause some notable (amplitude > 1 m) surface waves [Hayes, 2016]. Some anomalously scattering surfaces have been observed in the northern hemisphere's mares later in the mission, with these observations beginning in the northern spring [Hofgartner et al., 2016]. These anomalous scatterers could be interpreted as waves, but another leading explanation is that they are nitrogen-ethane bubbles separating from the lake's methane-ethane mixture [Hayes, 2016]. In any case however, wave features are not the norm.
- *Labyrinth:* We classified the labyrinths as forested ridges of about 150 m in height (not that we expect there to be forests on Titan) because the labyrinth terrain demonstrates a wide range of valley spacings and ridge widths, but lacks ridge heights tall enough to compare to the mountain ranges [Lopes et al., 2019]. In this case, the classification of the labyrinths as forested terrain may overestimate the terrain's characteristic roughness length. We chose to classify it as forested terrain, however, because some overestimation is not undesirable given that it will again likely assist us in creating an upper bound of possible surface heterogeneity.

To finish our map of roughness lengths and avoid over-emphasizing differences between regional values which are themselves only educated guesses, we rounded each value to the nearest order of magnitude before creating the final map.

4. *Topography:* We chose a map which uses radial basis functions to interpolate the relatively sparse elevation data available for Titan [Corlies et al., 2017]. As published, the maps don't include the flat surfaces of almost any of Titan's methane lakes and seas, so we corrected the surfaces by overwriting the elevation values of the four largest bodies of methane with the minimum elevation value seen along each of their coasts. Corlies et al. (2017) included the correct elevation of Ligeia Mare. Helpfully, Ligeia Mare, Punga Mare, and Kraken Mare are thought to be connected by subsurface hydrology and to thus have elevations within a few tens of meters of one another [Hayes et al., 2017]. Accordingly, we rewrote the elevations of Punga Mare and Kraken Mare to be the same as that of Ligeia.

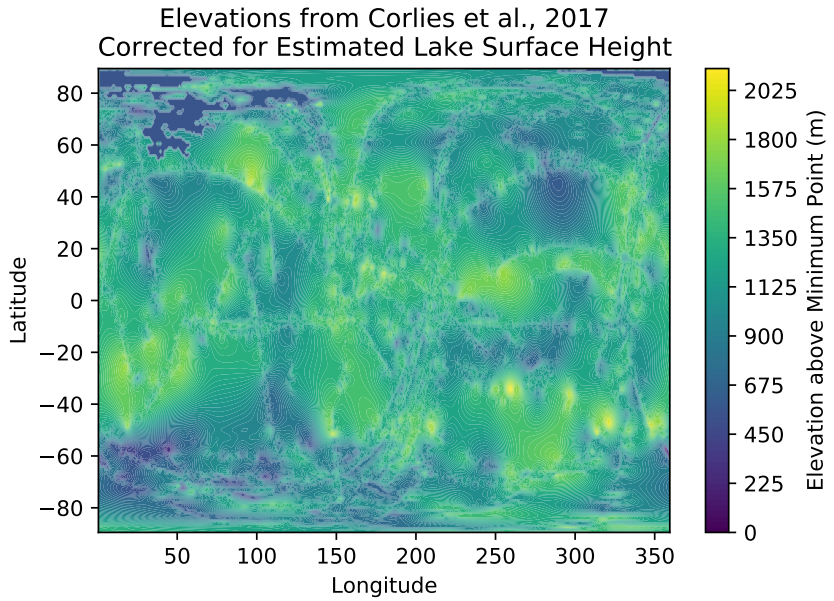

Figure 4: Topography Corrected for Estimated Lake Suface Height

In addition to any modifications specified above, the only changes made to previously published raster maps before their inclusion were re-gridding (only ever moving from higher resolution to lower resolutions) and, if necessary, the filling of a few (at most tens) of missing values with averages of their nearest real-value neighbors.

2.2 Model Initialization

TAM is a three-dimensional Titan GCM. Within the scope of current GCMs, it is of "intermediate complexity," meaning that it resolves or parameterizes the most important atmospheric processes but may not do so with high complexity (relative to some Earth climate models). Examples of the processes which TAM parameterizes are thermal properties, the exchange of radiative energy, the exchange of angular momentum in the boundary layer, and precipitation [Lora et al., 2015]. Dynamic subsurface hydrology was added in 2019 [Faulk et al., 2020]. We used TAM in its "T21" resolution (64 longitude points by 32 latitude points), with 48 atmospheric vertical layers and a time step of 600 seconds. For a control run, we also performed a spin-up run that lacked topography but was otherwise identical to the other runs. Each spin-up run entailed running TAM until it developed regular climate patterns. Once we had TAM spun-up, we could then use the atmospheric state at the end of the spin-up period as a starting point for model runs with maps of roughness lengths or albedo. We determined that the model's atmospheric and hydrological processes were spun-up after approximately 150 Titan years. We then used our spun-up atmospheric states to initialize the six further model runs that we actually analyzed:

1. Topography
2. No Topography (Control)
3. Roughness Lengths
4. Roughness Lengths and Topography
5. Albedo
6. Albedo and Topography

All six configurations were run for thirty Titan years. The quantities we recorded for study were the daily average of any specific quantity at any specific gridpoint, as well as the gridpoint's daily wind maxima and minima.

2.3 Preprocessing of Model Data and Brightness Temperature Observations

We focused our assessment of the model on two quantities – surface temperatures and near-surface winds – as befits our hypotheses. To assess surface temperatures, we compared

surface temperatures within the model to the surface brightness temperature observations collected by Cassini over the course of its mission (Jennings et al., 2019). We assessed each configuration's "skill" at forecasting surface temperatures by calculating skill scores as described in Hargreaves et al. (2013). These scores are designed to quantitatively compare the predictions of a model with actual observations. We calculated two sets of skill scores: one with the observations used being just the brightness, and one with the brightness temperatures corrected with an estimated emissivity of the surface at the brightness temperatures' wavelength. (Jennings et al. (2019) assumed an emissivity of 1 when they calculated brightness temperatures.) To estimate the emissivity of the surface at the 19 µm used by Jennings et al. (2019), we applied Kirchoff's Law to the 5.01 µm albedo measurements of Solomonidou et al. (2018). To finish correcting the brightness temperatures, we then used the fact that $I_{\lambda,T_b} = \epsilon I_{\lambda,T}$ if the brightness temperature has been calculated assuming that $\epsilon = 1$, and inverted Planck's law to get the relationship:

$$T = \frac{h\nu}{k} \ln^{-1}\left[1 + \epsilon\left(e^{\frac{h\nu}{kT_b}} - 1\right)\right] \tag{2}$$

where ϵ is the emissivity of the surface, T is the corrected surface temperature, T_b is the surface brightness temperature (itself calculated asssuming $\epsilon = 1$), k is Boltzmann's constant, h is Planck's constant, and ν is a frequency (Hapke, 2012). As the models are able to cover many Titan years while the observed temperatures span only about half a Titan year, we limited the modeled values to those in the observational time period.

To assess surface winds, we examined a number of different quantities. We calculated the per-terrain mean and standard deviation for the daily mean meridional and zonal wind components. We also performed the same calculations for the daily maximum and minimum of the zonal and meridional wind components. We scaled speeds at the model's lowest grid point (located at roughly 26 m above the surface) down to speeds at 10m using the logarithmic wind profile law, which provides a relationship between speeds at two different heights:

$$u\left(z_2\right) = u\left(z_1\right) \frac{\ln\left(\left(z_2 - d\right)/z_0\right)}{\ln\left(\left(z_1 - d\right)/z_0\right)} \tag{3}$$

where u_1 is the wind speed at height z_1. We also assumed that $d = 0$ because the elements on which d depends are too small to appear in any of the data on Titan's surface beyond the Huygens landing site.

3 Results

3.1 Surface Temperatures

Under the skill score formula of Hargreaves et al. (2013), skill scores range between -1 and 1. A score of 0 can be interpreted as stating that the model is as effective at forecasting as a constant value would be. Negative scores mean the model is worse than that constant value; positive values mean it is better, with 1 meaning the model predicts the observed values perfectly [Hargreaves et al., 2013]. The formula of Hargreaves et al. (2013) is as follows:

$$S = 1 - \sqrt{\frac{\sum (m_i - o_i)^2 - \sum (e_i)^2}{\sum (n_i - o_i)^2 - \sum (e_i)^2}} \tag{4}$$

where S is the score, m is the model's value, o is the observed value, n is a reference value (we chose this to be the mean of the observed values), and e is the error of the observation.

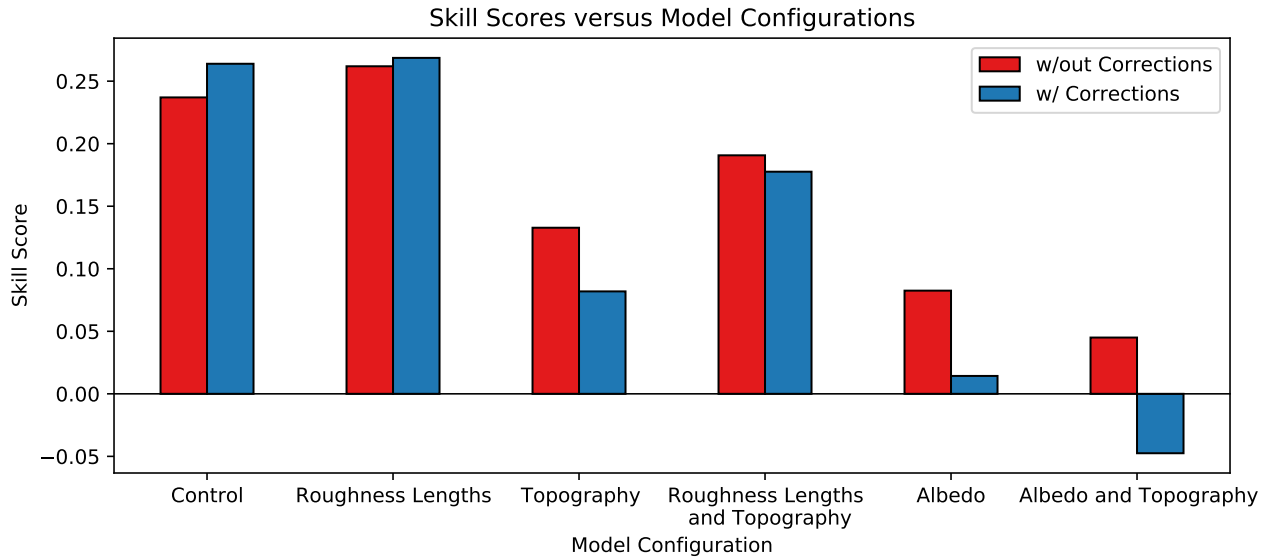

Figure 5: Surface Temperature Skill Scores

Given the distance between the wavelength of the observations in Jennings et al. (2019) and Janssen et al. (2015) (19 µm and 2.2 cm, respectively), we thought it best to present both skill scores calculated from Jennings et al.'s original brightness temperatures and those calculated from the surface temperatures which we had corrected for Titan's average zonal

emissivity (at 2.2 cm). Contrary to our first hypothesis, it appears that the model configurations with greater amounts of information on the surface are not generally better at predicting surface temperatures. The configuration with roughness lengths is (slightly) better than the control, but every other value configuration is worse. The skill score calculated using uncorrected surface brightness temperatures for the albedo and topography configuration is even negative, meaning that it's a worse prediction than the simplest possible surface temperature model (e.g. an average of our observations).

To gain a sense of surface climates within the model, as well as how those surface climates compare to the observations of Jennings et al. (2019), we computed yearly climatologies and compared them to the observations of Jennings et al. (2019).

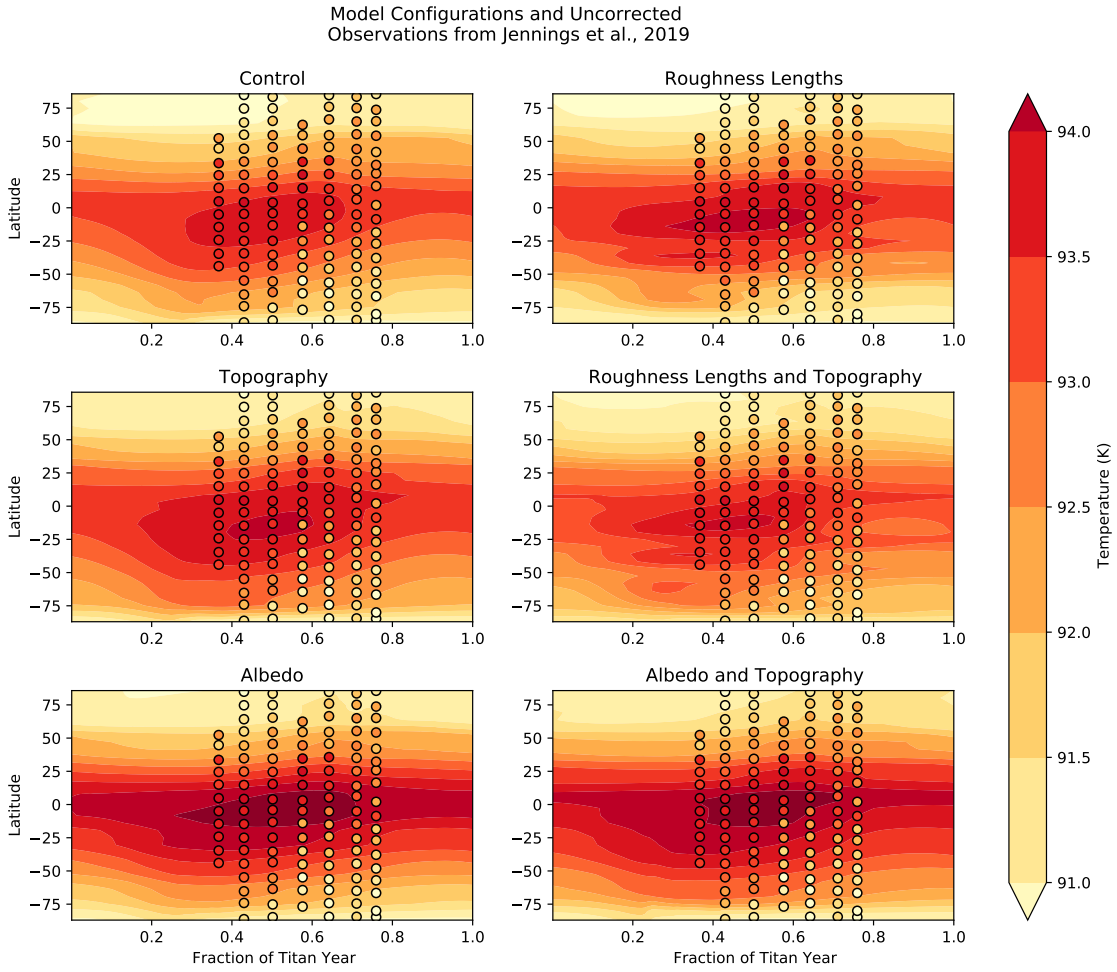

Figure 6: Surface Temperature Climatologies
Here, our Titan years start at the Southern Hemisphere's vernal equinox

In these, surface temperatures in the configuration with roughness lengths are mostly lower than those in the control, though the roughness length run is slightly warmer than the control towards the poles. Mean surface temperatures in the configurations with albedo, on the other hand, are all higher than those in the control.

To assess surface temperatures across various configurations and terrains, we computed both the per-terrain and the global means, maxima, minima, and standard deviations, which are plotted below. In the plots, the means and standard deviations have been computed after weighting them by the cosine of their latitude. The maxima and minima are the maxima and minima of the mean daily surface temperature.

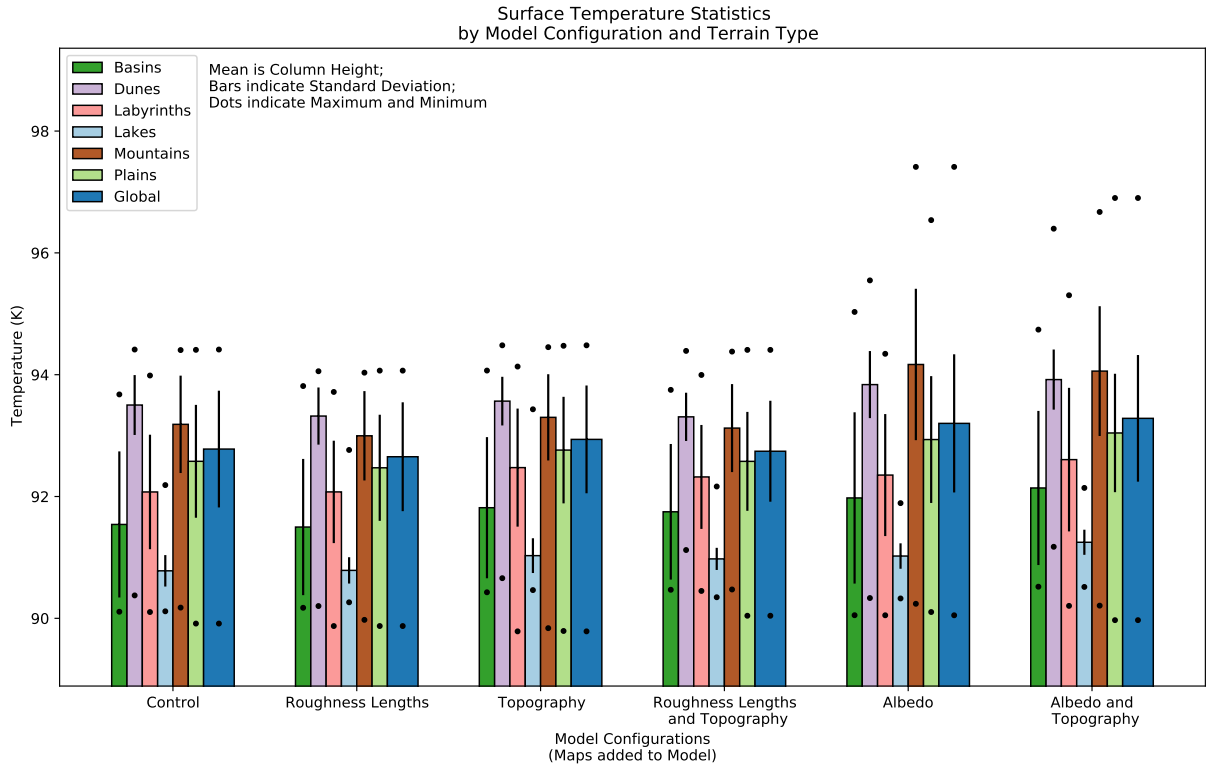

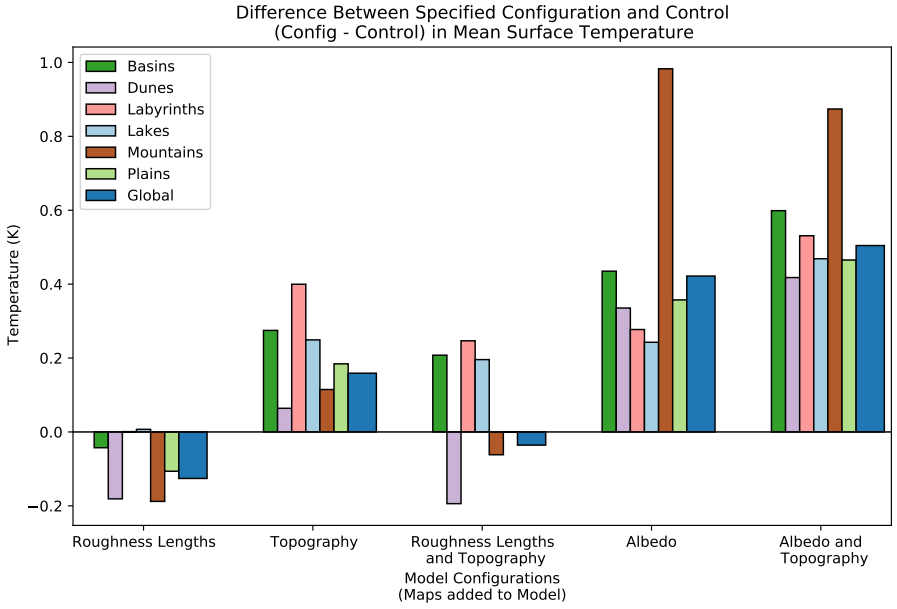

Figure 7: Daily Surface Temperature

Means and standard deviations have been computed after weighting the modeled values by the cosine of their latitude. The maxima and minima are the maxima and minima of the mean daily surface temperature.

In these plots, it is even more apparent that the mean temperatures of the albedo runs are higher than those in the control. More subtly, we can also see that the same inter-terrain trends in surface temperature hold from model configuration to model configuration. Additionally, deviations from the control seem to add somewhat linearly, as can be seen when comparing the differences from the control for the roughness lengths, topography, and roughness lengths *and* topography configurations, or when comparing the differences from the control for the topography, albedo, and albedo *and* topography configurations. We should also note that the average of the plains and the dunes, when combined, seems to dominate the global means.

3.2 Low-Level Winds

We began our analysis of low-level winds by testing our second hypothesis – that including heterogeneous roughness lengths in the model would modify wind speeds over Titan's seas. We thus started by examining the statistics of low-level winds over each of Titan's three seas: Kraken Mare, Ligeia Mare, and Punga Mare (listed from largest to smallest in terms of area).

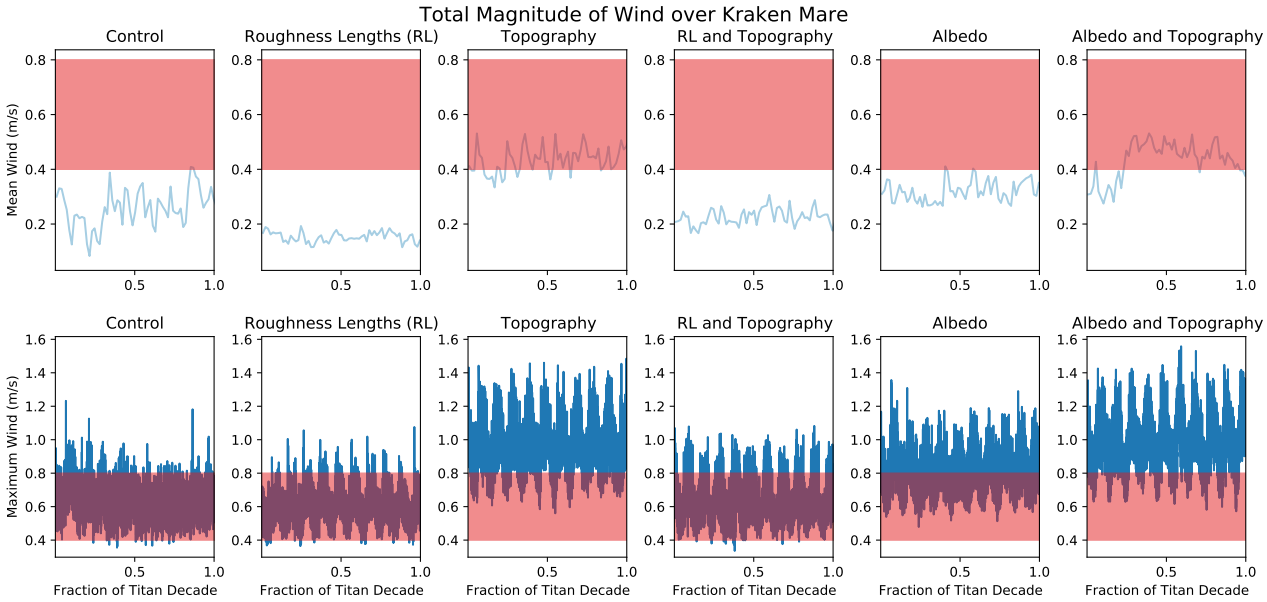
Total Magnitude of Wind over Kraken Mare
Control
Roughness Lengths (RL)
Topography
RL and Topography
Albedo
Albedo and Topography
Mean Wind (m/s)
Maximum Wind (m/s)
Fraction of Titan Decade

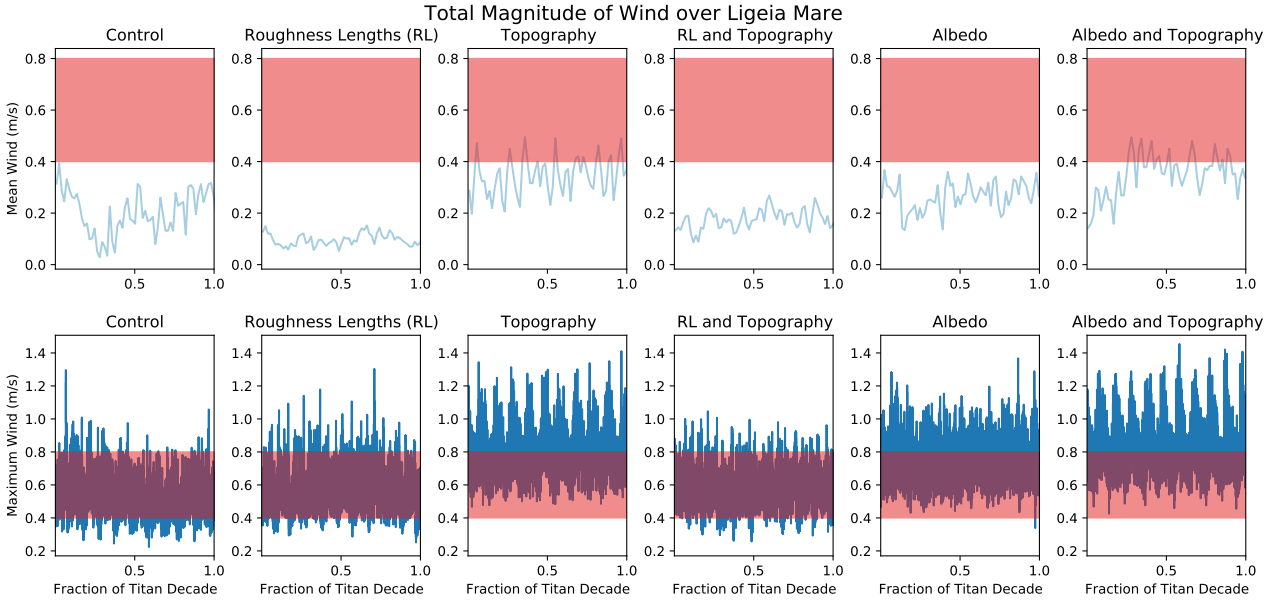
Total Magnitude of Wind over Ligeia Mare
Control
Roughness Lengths (RL)
Topography
RL and Topography
Albedo
Albedo and Topography
Mean Wind (m/s)
Maximum Wind (m/s)
Fraction of Titan Decade

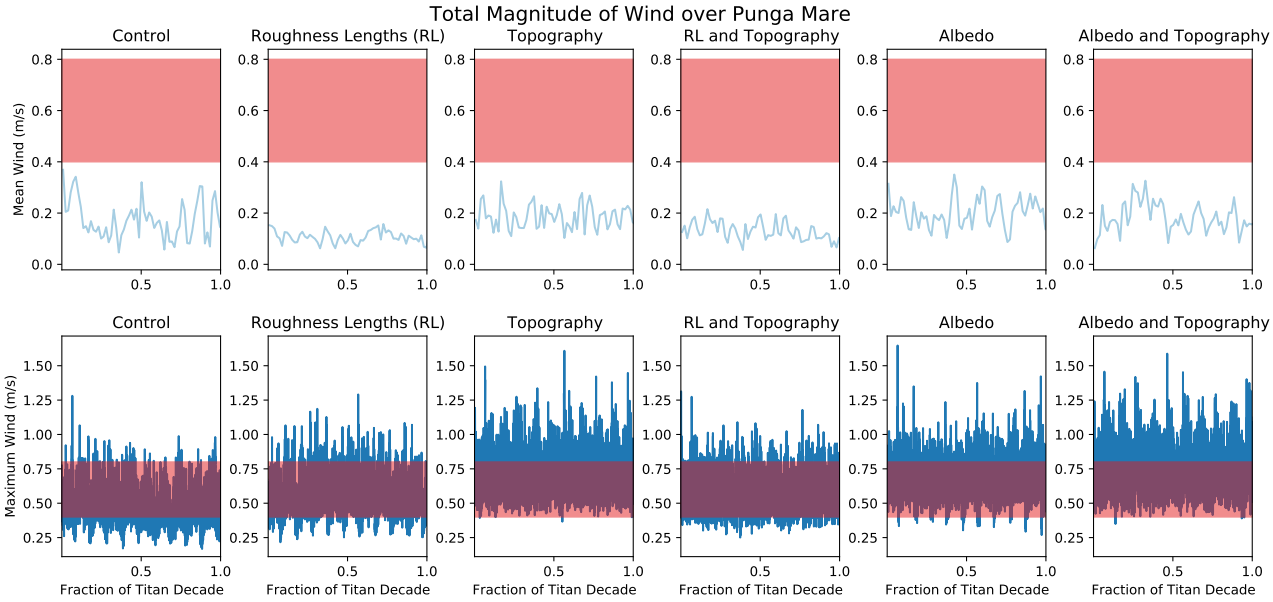

Figure 8: Mean of Daily Mean and Daily Maximum Wind Magnitudes over Seas
The red regions are the wind speeds identified as thresholds for wind-driven surface wave generation by Hayes et al. (2013). The lower boundary of the shaded region corresponds to the threshold necessary for a lake of pure methane; the upper to the threshold necessary for a lake of pure ethane.

We found that for the total magnitude of the wind (the model's meridional and zonal wind components combined using the Pythagorean theorem), the daily maximum of the total wind magnitude was high enough to produce wind-driven surface waves according to the thresholds of Hayes et al., (2013) over all the seas and in all the model configurations. Whether or not the magnitude of the mean wind daily wind reached the threshold from Hayes et al. was more complicated, however. Over Kraken Mare, the daily mean of wind magnitude was often within the threshold from Hayes et al. in the case of the configurations with topography, or albedo and topography. The daily mean of the wind magnitude in the configuration with just albedo was also high enough to just barely break the threshold region's lower boundary (0.4 m s^{-1}, corresponding to a lake of pure methane) during two (very short) periods. Over Ligeia Mare, the daily mean of the wind magnitude was again often within the threshold of Hayes et al. (2013) in the case of the configurations with topography, or albedo and topography. The configuration with albedo also again (just barely) broke the threshold region's lower bounds during one period lasting only a few days. Over Punga Mare, the daily mean of the wind magnitude breached the threshold region during only one period, which was on the order of one Titan year.

We also examined the zonal and meridional components of the modeled wind. We found that the daily mean zonal winds were lower than the threshold of Hayes et al. (2013) over all the seas and in all the configurations, but both eastward and westward daily maxima were always sufficiently high. The means and maxima of the meridional wind components present a more complicated situation. They were usually about twice the speed of the zonal winds, and the meridional component also did possess a number of cases where the daily mean was sufficient to land within the threshold of Hayes et al. (2013). There were also a number of cases where the mean daily maximum of the westward wind component was too low to breach the threshold of Hayes et al.

Over Kraken Mare, the mean daily meridional wind was high enough to breach the threshold (with mean daily winds spending as much as 50% of the decade 25% above the lower boundary of the region) in the configuration with topography, as well as the configuration with albedo and topography. The eastward daily maximum was often higher than the threshold's midpoint (0.6 m s^{-1}) in all the model configurations.

Over Ligeia Mare, the configuration with topography saw the daily mean of its meridional wind component breach the lower bound of the threshold (though by only 5% of the total threshold height at its greatest extent). The configuration with both albedo and topography saw the daily mean of its meridional wind component extend significantly into the threshold region (extending across nearly 50% of the threshold's total height) a number of times, for a total time of a bit over one Titan year spent above than the threshold's lower bound (i.e. greater than 0.45 m s^{-1}). The daily maxima of the westward component spent only very limited periods of time (>5% of a Titan decade) in the threshold region, and even then only rarely breached the midpoint of the region. In the configuration with both roughness lengths and topography, the daily maximum of the westward component never breached the lower bound of the region.

Over Punga Mare, the mean daily meridional wind component was never high enough to breach the threshold region. In all configurations, the daily maximum of the eastward wind component did occasionally break the threshold, and the westward component also often broke the threshold. The only configuration where the daily maximum of the westward wind was not often above 50% of the threshold region was the control run.

To further examine low-level winds, we calculated the same statistics as in our examination of surface temperatures, but we calculated them for three different wind components: the zonal wind, the meridional wind, and the magnitude of the vector formed by those two components. In our calculations of the mean and standard deviation, we again weighted

winds by the cosine of the latitude of each observation's gridpoint. (In this case, The mean winds were roughly within the interval 0.1-0.5 m s^{-1} and the standard deviation were within 0.05-0.3 m s^{-1}. The maxima were roughly within 0.5-1.5 m s^{-1}.) We again weighted our calculations of the mean and standard deviation by the cosine of each gridpoint's latitude.

We found that the lakes and basins had the highest mean wind magnitudes, while the dunes and mountains had the lowest. The relative positions of some of the mean magnitudes changed as well, with the means of the wind magnitude in the mountains and labyrinths varying their positions relative to the other terrains by the greatest amounts. The topography, albedo, and topography and albedo configurations generally saw the highest mean wind magnitudes. Likewise, the largest differences from the control in the per-terrain and global means were seen in those same three runs.

For the zonal wind, we found that the highest per-terrain mean zonal winds were seen in the control and albedo configurations, though the largest variation (as measured by the standard deviation over each terrain) was actually seen in the configurations with topography, or roughness lengths and topography. Generally, the control configuration saw per-terrain mean zonal winds which were higher than those in any of the other configurations. (The configurations with roughness lengths or albedo formed partial exceptions to this trend.)

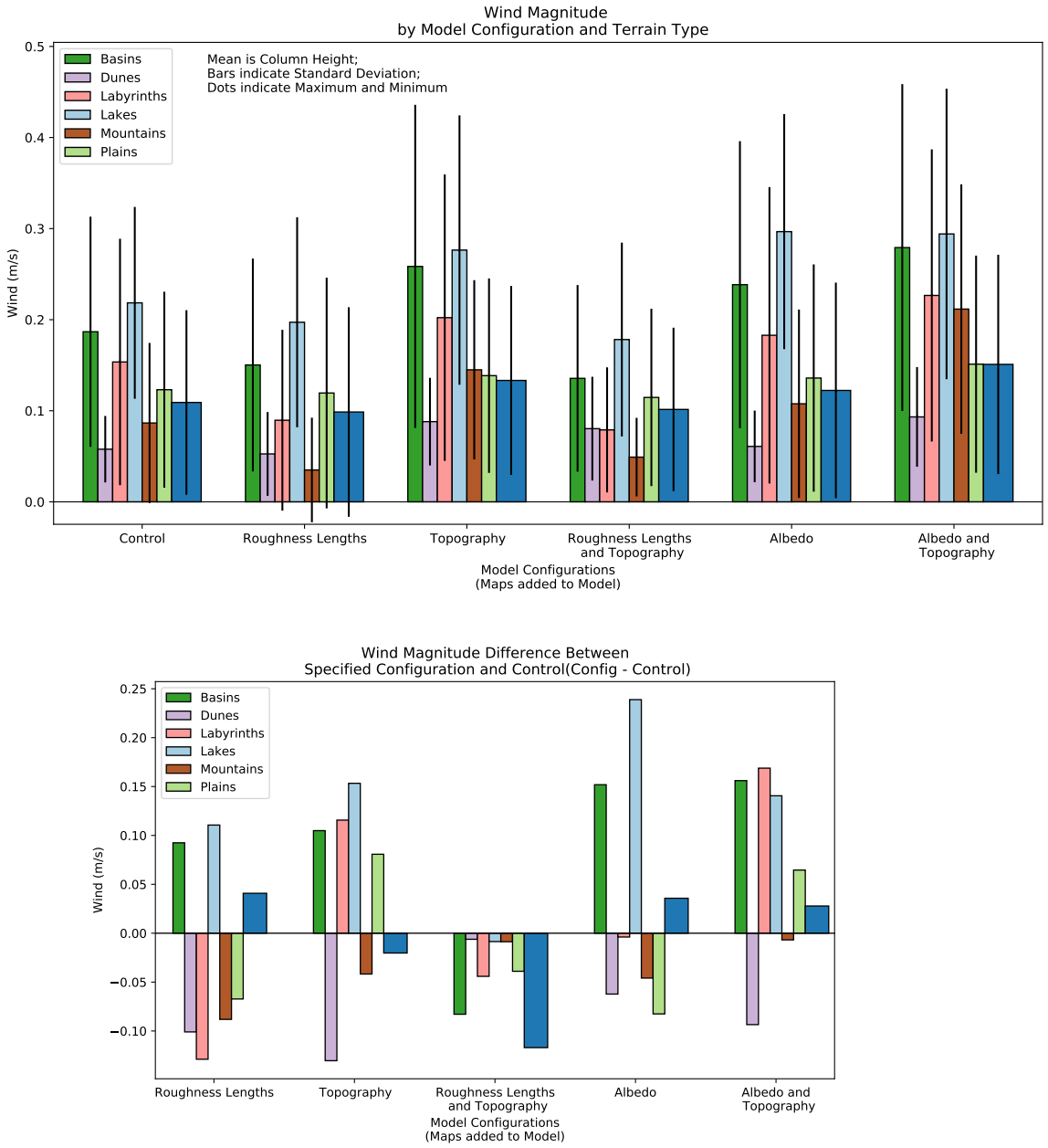

Figure 9: Wind Magnitude Statistics by Terrain and Model Configuration
Magnitudes were calculated by applying the Pythagorean theorem to the diurnal mean of the meridional and zonal wind components.

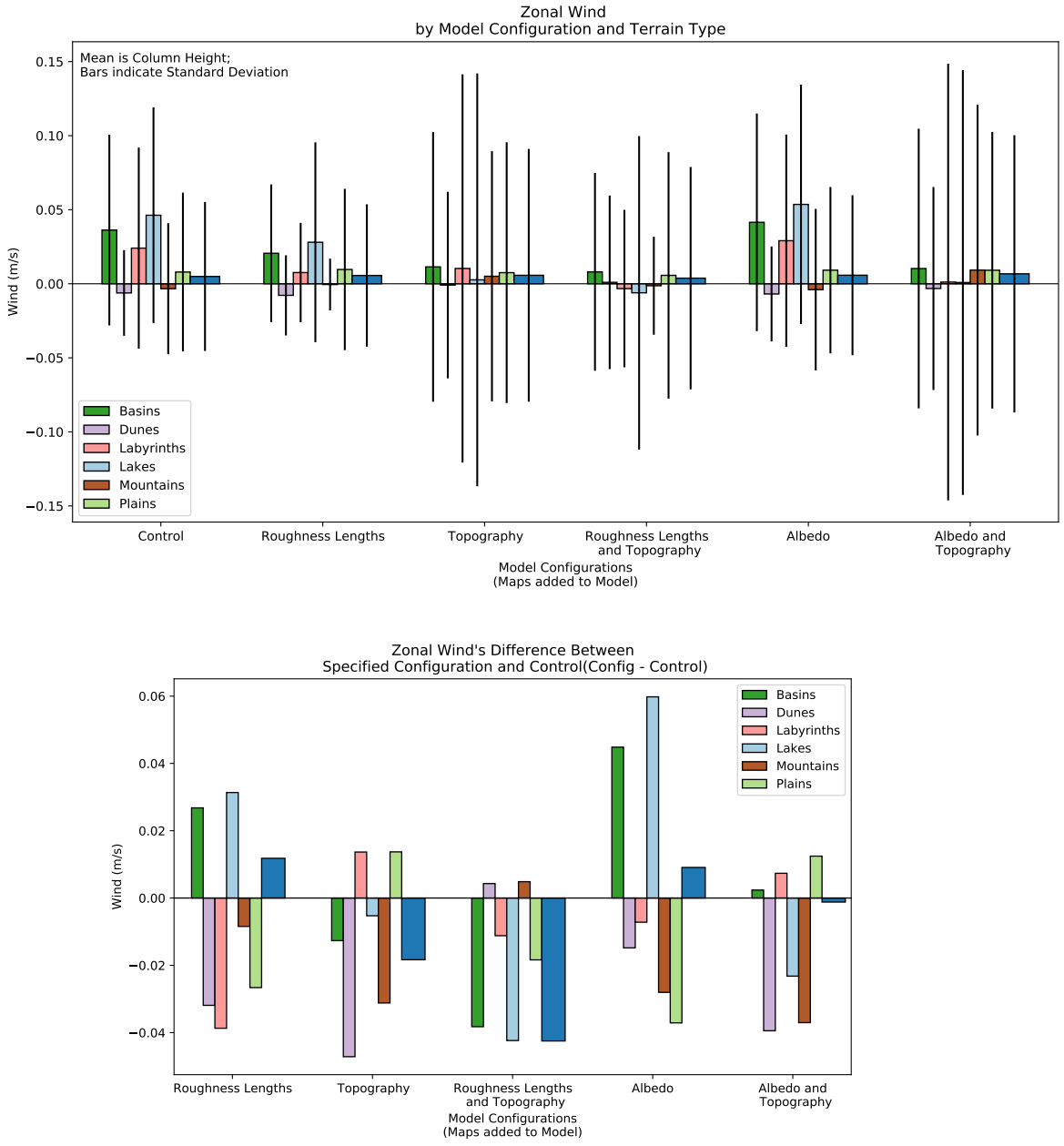

Figure 10: Zonal Wind Statistics by Terrain and Model Configuration
Negative Values indicate westward winds; positive values eastward winds

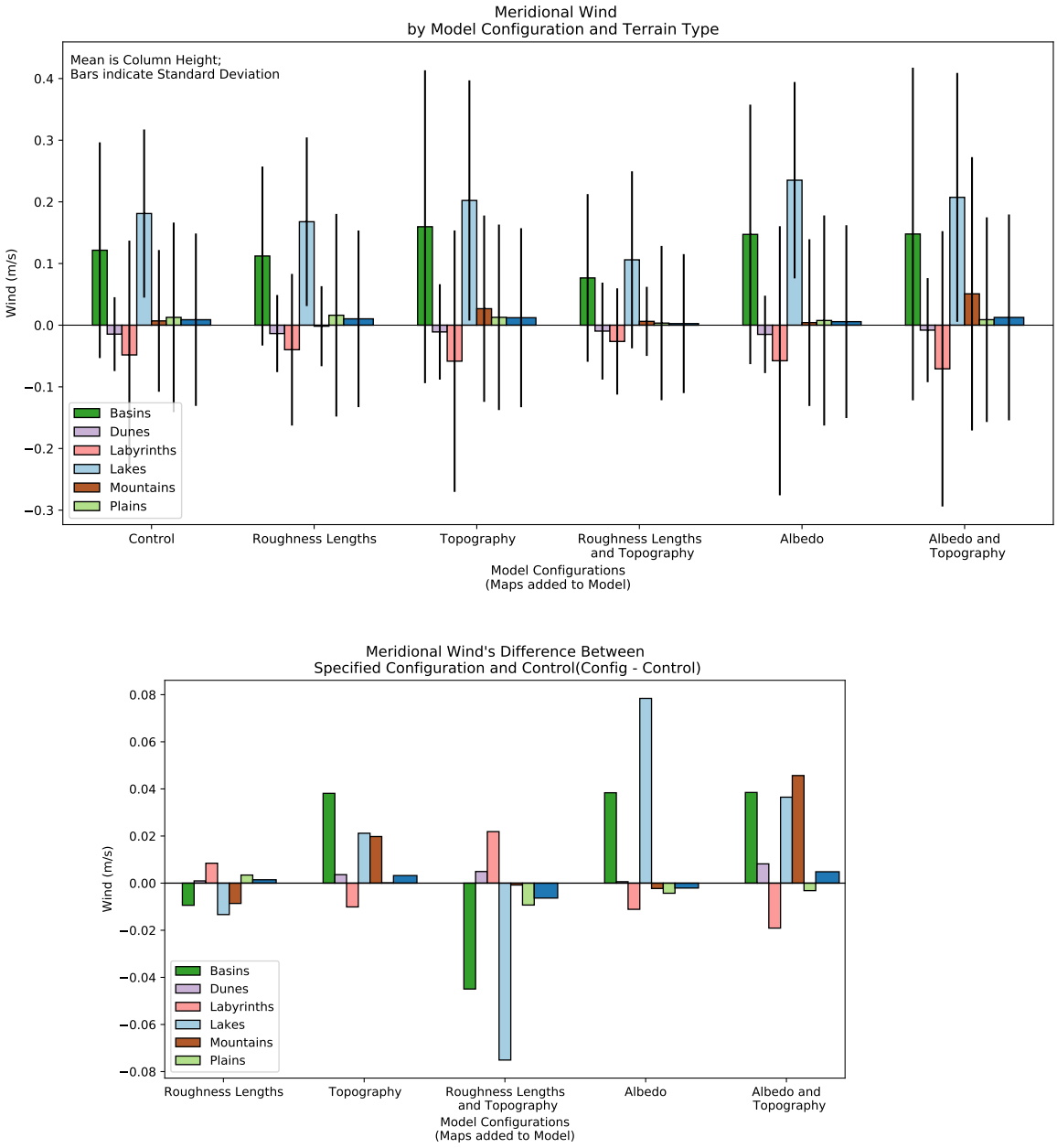

Figure 11: Meridional Wind Statistics by Terrain and Model Configuration
Negative Values indicate southward winds; positive values northward winds

For the meridional wind, we found that the per-terrain mean winds were highest over the lakes and the basins, with lakes seeing the highest mean meridional winds overall. The highest per-terrain standard deviations likewise occurred over the lakes and basins. The largest differences from the control were seen over the lakes and the basins. The configuration with

only heterogeneous albedos saw the highest meridional wind speeds over the lakes, while the configurations with topography, or albedo and topography, had similarly high (relative to the other configurations) above-lake meridional wind speeds.

4 Discussion

4.1 Surface Temperatures

4.1.1 Skill Scores

I would argue that much of the tendency for the configurations with heterogeneous surface boundary conditions to have lower skill scores is best explained by examining the individual surface temperature responses elicited by each type of heterogeneous boundary condition.

An examination of figure 6 shows that the variation from the control in the per-terrain mean surface temperatures is lowest (on a terrain-by-terrain basis) in the case of the configuration with only heterogeneous roughness lengths. The difference between the global means of the control configuration and the global means of a heterogeneous configuration is actually lowest in another configuration – that with roughness lengths and topography – but unlike the configuration with just roughness lengths, the configuration with both roughness lengths and topography had per-terrain differences from the control which were both positive and negative. It appears that this very low difference in the global means of the control configuration and the configuration with both roughness lengths and topography was due more to cancellation between positive and negative differences than an actually greater similarity between the roughness lengths and topography configuration and the control configuration (with this greater similarity relative to the configuration with just roughness lengths).

Examining the variation between the control configuration and a heterogeneous configuration by focusing on the differences in per-terrain means, rather than the differences in global means, seems to show that a greater amount of per-terrain difference from the control generally leads to lower skill scores. This is what we would expect under the structure of the skill score formula of Hargreaves et al. (2013). What is more difficult to explain, however, are the reasons behind the surface temperature responses seen in each model configuration, and the way most of the surface heterogeneities seem to push the model further, rather than closer, to observations.

I believe that it is possible to argue that the way the roughness lengths configuration produces slightly higher skill scores than the control in both sets of skill scores (those with

corrections and those without) is evidence of these roughness length estimates being at least somewhat "realistic" in their values and positioning in the final surface boundary condition data set. This line of thought may also imply that the other boundary condition data sets are less realistic than the control's assumption of homogeneity in certain quantities (like topography and albedo; the control configuration's albedo values are listed in Table 2 below). Instead of simply saying that one dataset is "less" realistic than a homogeneous surface, however, I would like to examine some reasons as to why we might see the surface temperature responses we found.

The roughness length response seems the most difficult to explain, as it ties into the relationships of low-level wind patterns and speeds, and thus affects surface temperatures only indirectly. In the case of the heterogeneous albedo and heterogeneous topography configurations, it is somewhat easier to offer an possible explanation.

Regarding topography, the dataset for heterogeneous topography exhibits the strong asymmetry in elevations that has been previously remarked upon [Tokano, 2019; Corlies et al., 2017].

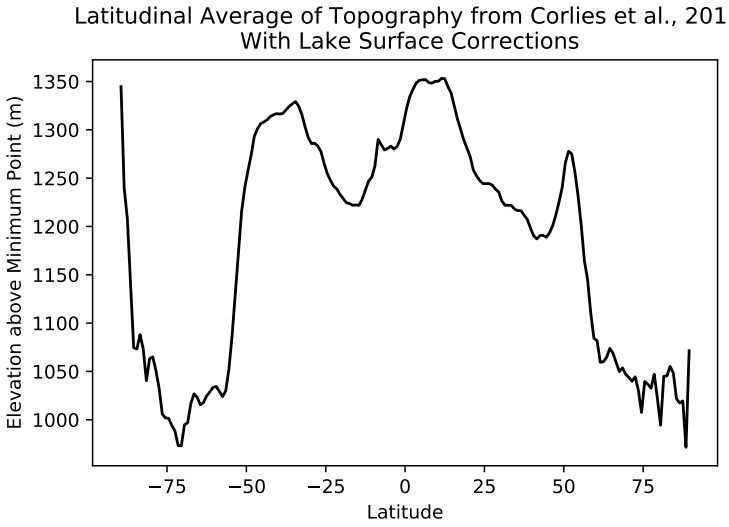

Figure 12: Latitudinal Average of Elevations in Heterogeneous Topography Dataset

Though the relative importance of this asymmetry against other climatic asymmetries, such as those in Titan's orbital parameters, remains somewhat uncertain, it's likely that the topographic asymmetry plays an important role in confining methane – and thus moist processes – to the polar regions, particularly those near the north pole [Tokano, 2019]. The simple fact that the polar regions are lower in the configurations with heterogeneous

topography than in those without it could also explain why we saw somewhat higher near-pole surface temperatures in the heterogeneous topography runs.

Regarding albedos, the heterogenenous albedo dataset has a lower effective albedo than the control run, largely because we estimated that the albedos of the terrains near the equator, where insolation is most readily absorbed, were lower than that in the control. This would increase the overall amount of energy available to the surface-atmosphere system, and drive up surface temperatures and, possibly, winds.

Radiative Transfer Regime	**Heterogeneous Dataset**	**Control**
Solar-Wavelength	0.2154	0.25
Thermal Infrared	0.0252	0.05

Table 2: Global Means of Albedo in Heterogeneous Dataset and Control
Each albedo value was weighted by the cosine of that value's latitude.

This could explain the majority of the the way the configurations with albedo see higher surface temperatures than the control. The case of the configurations with topography is, like that of roughness lengths, also more difficult to explain. It is curious that every terrain type has a mean which is higher in the topography configuration than in the control run.

4.1.2 Linearity in Surface Temperature Responses

One phenomenon apparent in the model's response to hetereogeneous surface boundary conditions is the way that the differences in per-terrain mean surface temperatures add somewhat linearly. The reasons behind this are somewhat complex, given that they involve interactions between multiple heterogeneous surface boundary conditions, but I would like to note that in both cases where a linearity in responses can be examined, we can see that the full model run has exhibits a difference from the control that's slightly lower than what a simple addition of "one reponse + the other" would predict. I would argue that some of the reason for why we see this linearity only in surface temperatures, rather than surface temperatures and wind, is that wind is generally a more nonlinear, chaotic system.

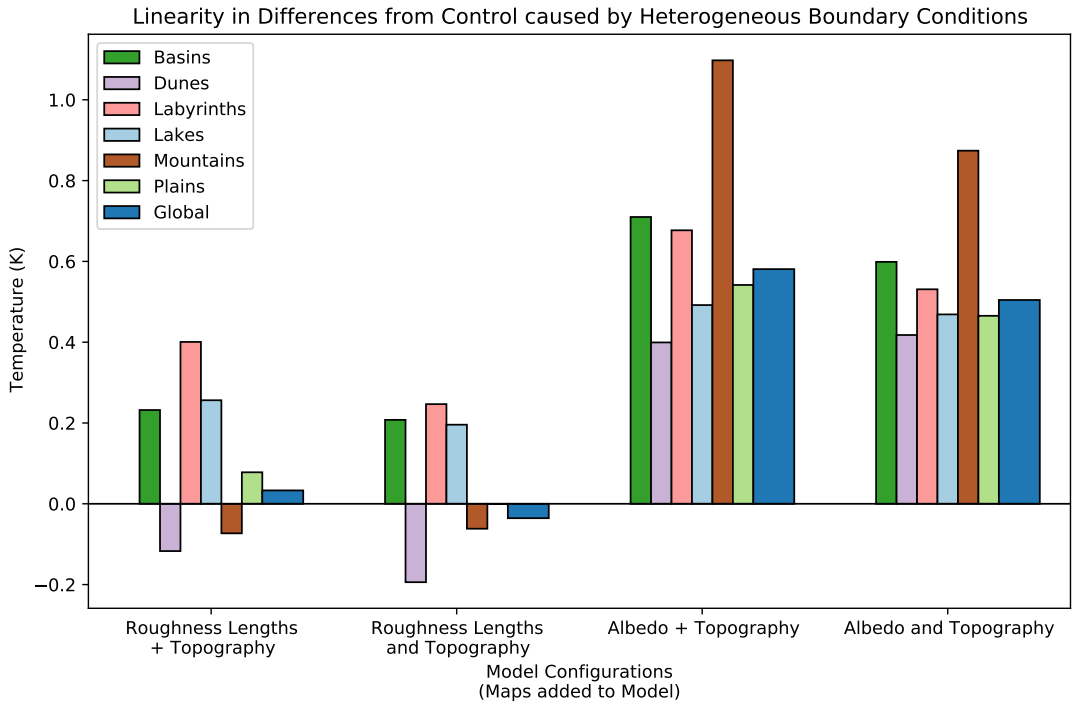

Figure 13: Linearity in Surface Temperature Response

The plots with "+" in their descriptions are those which were produced by adding the (config-control), with "config" and "control" the mean for their respective configurations, for one configuration to the (config-control) for another configuration. The plots with "and" refer to the configurations which had multiple maps used in the model at once.

4.2 Surface Winds

4.2.1 Near-Surface Winds Over Titan's Seas

When it comes wind-driven surface waves on Titan's seas, two things that are of relative importance to note are that the threshold of Hayes et al. (2013) is dependent on the methane-ethane composition of the lake, and that there are a number of other factors which play into the ability of Titan's seas to develop wind-driven surface waves at any particular wind speed. Regarding sea compositions, Kraken Mare is thought to be roughly 70% methane, 16% nitrogen, and 14% ethane [Poggiali et al., 2020]. Ligeia Mare is thought to be 71% methane, 17% nitrogen, and 12 % ethane [Hayes, 2016]. Punga Mare is thought to be 80% methane and almost 20% nitrogen, with a negligible amount of ethane [Mastrogiuseppe, 2018]. These compositions have implications for the use of the threshold from Hayes et al. (2013) in

assessing the presence of surface waves. Specifically, they imply that Punga Mare may not experience surface waves as regularly as Kraken Mare and Ligeia Mare, as the mean wind magnitude only extends into the threshold once (for a limited period in the configuration with topography and albedo), and does not seem to extend into the threshold far enough to surpass the magnitude of roughly 0.48 m s^{-1} which would be required for a lake that of about only 80% methane. (This threshold is of course an estimate, as it doesn't appear that Hayes has yet taken into account the effects of the nitrogen mixed into the seas.) However, even Punga Mare does see the maximum daily wind magnitudes break the threshold speeds by a margin which would seem to guarantee surface waves under the threshold of Hayes et al. Another important caveat to this work is the fact that there remains debate on the possibility of aerosol products and related surface films damping surface waves, and thus possibly explaining some of remarkably-calm seeming sea surfaces observed by Cassini [Cordier and Carrasco, 2019]. The threshold range we used does not take this into account, and would likely need to be significantly higher over bodies of methane covered with films.

We found that the seas saw significantly lower wind speeds (both zonal and meridional) in the configurations with heterogeneous roughness lengths. This was not what we expected, as the surface roughness lengths we assigned to the sea surfaces themselves were significantly lower than the roughness length used in the control configuration (0.005 m), but it is possible that the the mountain and labyrinth terrains, which border much of the seas' coastlines and have much higher roughness lengths (1 m), could have suppressed the effect of the lower roughness lengths over the seas themselves.

An additional point of note is that in all configurations Punga Mare generally saw lower wind speeds than Kraken Mare or Ligeia Mare. I would assert that this is likely due to Punga's position, which is at least 5° farther north than either of the other mares.

4.2.2 Per-Terrain Variation in Near-Surface Winds

When comparing the per-terrain meridional wind, or wind magnitude, the relative position of the lakes and basins, as the terrains with by far the fastest mean winds, warrants at least some explanation. Much of this is due to these terrain's positions relative to the other terrains. The lake and basin terrains have the vast majority of their grid points much closer to the poles than the other grid points, and the modeled near-surface winds are generally much stronger closer to the poles.

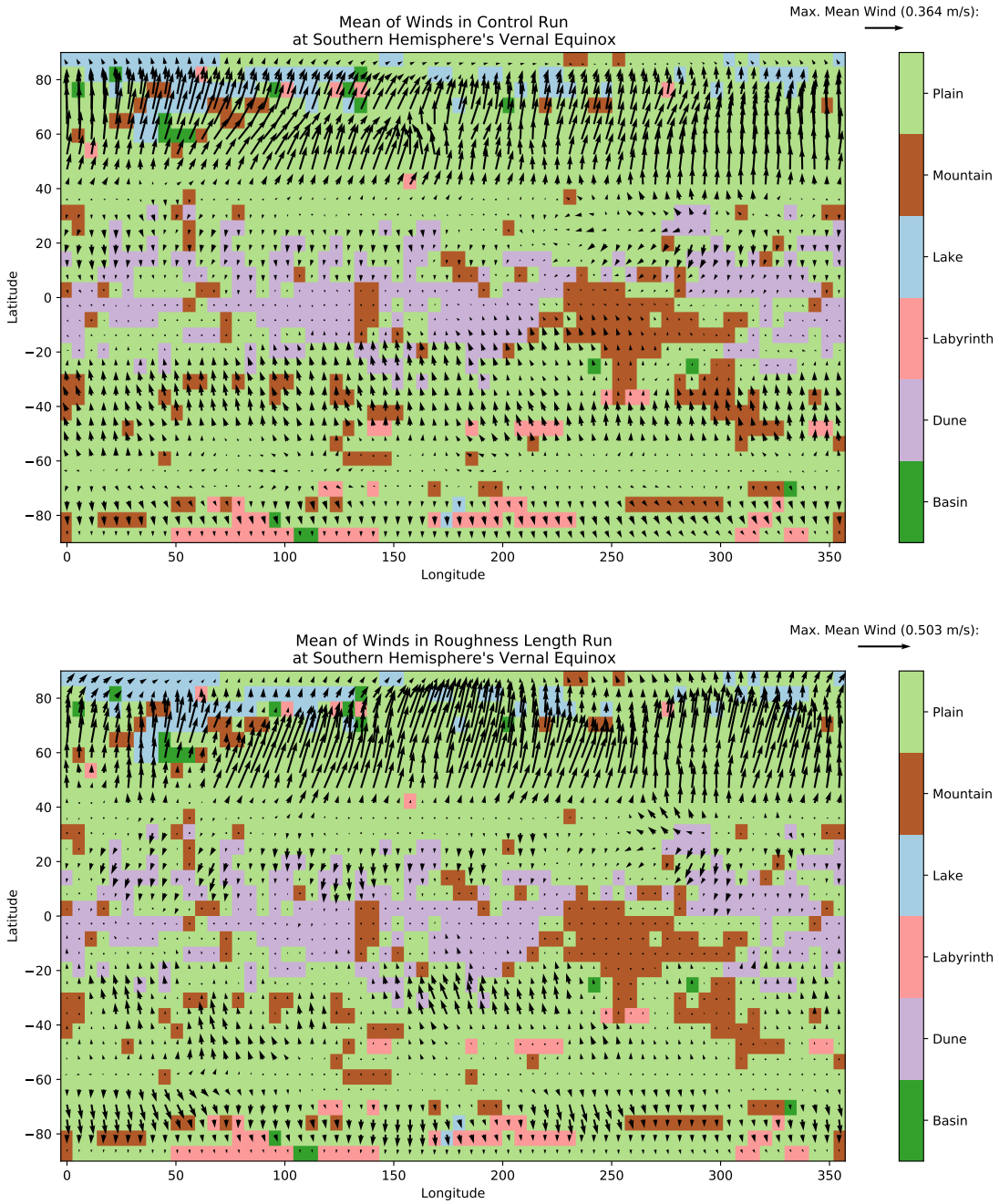

Figure 14: Quiver Plots of the Mean Winds in the Control and Roughness Length Configurations at the Southern Hemisphere's Spring Equinox, with Rasterized Terrain Classifications from Lopes et al., 2019

5 Summary

In this thesis, we assessed the impact of heterogeneous surface boundary conditions on Titan's near-surface atmosphere and climate. We did this by creating maps of Titan's topography, possible surface roughness lengths, and possible albedo, and using them in the Titan Atmospheric Model both separately and in two combinations. We had hypothesized that the inclusion of heterogeneous roughness lengths in TAM would cause the model to produce surface temperatures which better matched those observed in the thermal emissions analysis of Jennings et al. (2019). We found, however, that only the heterogeneous surface roughness lengths improved the model's fit, and they did that by a negligible amount (an improved skill score of roughly 5%), while topography and heterogeneous albedos both made the fit significantly worse (skill score decreases of as much as roughly 60%).

Using the terrain classifications of Lopes et al. (2019), we examined the per-terrain statistics for surface temperature. We found that the model exhibited a somewhat linear response in the way surface temperatures were affected by running the model with one or more heterogeneous surface boundary conditions. We also found that the surface temperatures in the model seemed relatively sensitive to changes in solar-wavelength albedo. One area of possible improvement and future work is a set of realistic albedo maps which leads to skill scores that match or exceed the skill scores of the control. Additional examination of the factors which caused the model configurations with topography to produce markedly worse skill scores might be another task for future study.

We also found that heterogeneous boundary conditions had a noticeable effect on modeled winds, both over Titan's seas and over Titan as a whole. The configurations with heterogeneous roughness lengths generally exhibited lower wind speeds over the seas than the control, even though the roughness lengths over the seas in the heterogeneous boundary conditions are significantly lower than those in the control. We attribute this to the way most of the seas are bounded by regions with terrains which have much higher roughness lengths than the control. We compared over-sea wind speeds to the wind-driven wave thresholds of Hayes et al. (2013), and found that the maxima of the wind magnitude were always sufficient to generate surface waves according to the threshold. The means of the configurations were not sufficient more often than they were sufficient, but the configurations with topography, or albedo and topography, often did see mean wind magnitudes which would seem enough to generate surface waves over Ligeia Mare and Kraken Mare. Punga Mare saw wind magnitudes which were almost always lower than those of Ligeia and Kraken Mare, and none of Punga's mean modeled wind magnitudes were sufficient to initiate waves according to the

Hayes et al. (2013) threshold.

This thesis contributes to the growing body of literature regarding the interactions between Titan's surface and atmosphere, but much work remains to be done on subject. One possible study which could use the surface boundary conditions developed for this thesis, or similar datasets, would be an examination of the surface-induced forcing of stationary waves, similar to the study of Garfinkel et al. (2020) for surface-heterogeneity-induced stationary waves on Earth.

Acknowledgements

This project has been under way, in one form or another, since early in the spring of 2020. I couldn't have finished it, or produced something with anywhere near this level of detail, without the assistance of an array of talented and kind individuals.

My thanks to Dr. Juan Lora for his time, expertise, patience, and continual good humor over the long process of this thesis's production. My thanks to Dr. Michael Battalio for his assistance in setting up and actually running TAM, and for all the helpful tips and suggestions he's provided while viewing the many different iterations of this project's results. My thanks to Dr. Mark Brandon for agreeing to read all of this and provide comments.

My thanks to my collaborator, thesis-twin and fellow outer-solar-system enthusiast Mary Yap for her humor, enthusiasm, and unfailingly high academic standards. She has been a great help in making my work all that it can be.

My thanks to Dr. Michael Janssen, Dr. Rosaly Lopes, and Ashley Schoenfeld at the Jet Propulsion Laboratory for their data, correspondence, and – in Ashley's case – valiant efforts to battle with VPN software and ensure that science could safely continue moving forward, even in the opening months of a major pandemic.

My thanks to Berkeley College, the Richter Family, and the Yale College Dean's Research Fellowship for funding my summer work.

My thanks to all the good folks who built Python's ecosystem of packages, the good folks at Yale who manage our (very powerful, surprisingly friendly and easy-to-use) computing clusters, and everyone whose data and papers I've referenced while writing this thesis.

Finally, I would like to thank my friends and family for their patience in listening to me talk about Titan, Python notebooks, and good (or bad) code. Viewing this project through outside eyes has been a great help in remaining motivated and excited about the work.

To me, Titan remains not only very cold, but also very cool. It's been an even more enjoyable place to work thanks to all the people above.

References

- (2019). Aerodynamic Roughness Length. Glossary of Meteorology, American Meteorological Society.
- (2019). Global Wind Atlas 3.0, Technical University of Denmark.
- G. Hayes, J. M. S., M. A. Donelan, and R. D. Lorenz (2017). Modeling and Observing the Role of Wind-Waves on Titan's Hydrocarbon Seas: Adding Anemometry to Cassini's Repertoire. Lunar and Planetary Science XLVIII
- Abd Razak, A., A. Hagishima, N. Ikegaya and J. Tanimoto (2013). "Analysis of airflow over building arrays for assessment of urban wind environment." Building and Environment **59**: 56-65.
- Achterberg, R. K., B. J. Conrath, P. J. Gierasch, F. M. Flasar and C. A. Nixon (2008). "Observation of a tilt of Titan's middle-atmospheric superrotation." Icarus **197**(2): 549-555.
- Achterberg, R. K., B. J. Conrath, P. J. Gierasch, F. M. Flasar and C. A. Nixon (2008). "Titan's middle-atmospheric temperatures and dynamics observed by the Cassini Composite Infrared Spectrometer." Icarus **194**(1): 263-277.
- Ahrens, C. D. (2010). Essentials of Meteorology: An Invitation to the Atmosphere, Cengage Learning.
- Battalio, M. and H. Wang (2019). "The Aonia-Solis-Valles dust storm track in the southern hemisphere of Mars." Icarus **321**: 367-378.
- Bézard, B., S. Vinatier and R. K. Achterberg (2018). "Seasonal radiative modeling of Titan's stratospheric temperatures at low latitudes." Icarus **302**: 437-450.
- Brossier, J. F., S. Rodriguez, T. Cornet, A. Lucas, J. Radebaugh, L. Maltagliati, S. Le Mouélic, A. Solomonidou, A. Coustenis, M. Hirtzig, R. Jaumann, K. Stephan and C. Sotin (2018). "Geological Evolution of Titan's Equatorial Regions: Possible Nature and Origin of the Dune Material." Journal of Geophysical Research: Planets **123**(5): 1089-1112.
- Cordier, D. and N. Carrasco (2019). "The floatability of aerosols and wave damping on Titan's seas." Nature Geoscience **12**(5): 315-320.
- Corlies, P., A. Hayes, S. Birch, R. Lorenz, B. Stiles, R. Kirk, V. Poggiali, H. Zebker and L. Iess (2017). "Titan's Topography and Shape at the End of the Cassini Mission." Geophysical Research Letters **44**(23): 11,754-711,761.
- Cottini, V., C. A. Nixon, D. E. Jennings, R. de Kok, N. A. Teanby, P. G. Irwin and F. M. Flasar (2012). "Spatial and temporal variations in Titan's surface temperatures from Cassini CIRS observations." Planetary and Space Science **60**(1): 62-71.
- Dalton, J. (2010). "Spectroscopy of icy moon surface materials." Space science reviews **153**(1-4): 219-247.
- Faulk, S., J. Mitchell, S. Moon and J. Lora (2017). "Regional patterns of extreme precipitation on Titan consistent with observed alluvial fan distribution." Nature Geoscience **10**(11): 827-831.
- Faulk, S. P., J. M. Lora, J. L. Mitchell and P. Milly (2020). "Titan's climate patterns and surface methane distribution due to the coupling of land hydrology and atmosphere." Nature Astronomy **4**(4): 390-398.
- Foken, T. (2006). "50 years of the Monin–Obukhov similarity theory." Boundary-Layer Meteorology **119**(3): 431-447.
- Friedson, A. J., R. A. West, E. H. Wilson, F. Oyafuso and G. S. Orton (2009). "A global climate model of Titan's atmosphere and surface." Planetary and Space Science **57**(14-15): 1931-1949.
- Garratt, J. R. (1977). "Review of Drag Coefficients over Oceans and Continents." Monthly Weather Review **105**(7): 915-929.
- Garratt, J. R. (1994). "The atmospheric boundary layer." Earth-Science Reviews **37**(1-2): 89-134.

References

- Gosse, S., D. Labrie and P. Chylek (1995). "Refractive index of ice in the 1.4–7.8-μm spectral range." Applied optics **34**(28): 6582-6586.
- Grima, C., M. Mastrogiuseppe, A. G. Hayes, S. D. Wall, R. D. Lorenz, J. D. Hofgartner, B. Stiles, C. Elachi and C. R. Team (2017). "Surface roughness of Titan's hydrocarbon seas." Earth and Planetary Science Letters **474**: 20-24.
- Grundy, W. M. and B. Schmitt (1998). "The temperature-dependent near-infrared absorption spectrum of hexagonal H2O ice." Journal of Geophysical Research: Planets **103**(E11): 25809-25822.
- Guan, C. and L. Xie (2004). "On the linear parameterization of drag coefficient over sea surface." Journal of Physical Oceanography **34**(12): 2847-2851.
- Gueymard, C. A. (2004). "The sun's total and spectral irradiance for solar energy applications and solar radiation models." Solar Energy **76**(4): 423-453.
- Halley, E. (1753). "An historical account of the trade winds, and monsoons, observable in the seas between and near the Tropicks, with an attempt to assign the physical cause of the said winds." Philosophical Transactions of the Royal Society of London **16**(183): 153-168.
- Hansen, F. V. (1993). Surface roughness lengths, ARMY RESEARCH LAB WHITE SANDS MISSILE RANGE NM.
- Hapke, B. (2012). Theory of reflectance and emittance spectroscopy, Cambridge university press.
- Hargreaves, J. C., J. D. Annan, R. Ohgaito, A. Paul and A. Abe-Ouchi (2013). "Skill and reliability of climate model ensembles at the Last Glacial Maximum and mid-Holocene." Climate Past **9**: 811-823.
- Hayes, A. G. (2016). "The Lakes and Seas of Titan." Annual Review of Earth and Planetary Sciences **44**(1): 57-83.
- Hayes, A. G., S. P. D. Birch, W. E. Dietrich, A. D. Howard, R. L. Kirk, V. Poggiali, M. Mastrogiuseppe, R. J. Michaelides, P. M. Corlies, J. M. Moore, M. J. Malaska, K. L. Mitchell, R. D. Lorenz and C. A. Wood (2017). "Topographic Constraints on the Evolution and Connectivity of Titan's Lacustrine Basins." Geophysical Research Letters **44**(23): 11,745-711,753.
- Hayes, A. G., R. D. Lorenz, M. Donelan, M. Manga, J. Lunine, T. Schneider, M. Lamb, J. Mitchell, W. Fischer and S. Graves (2013). "Wind driven capillary-gravity waves on Titan's lakes: Hard to detect or non-existent?" Icarus **225**(1): 403-412.
- Hayes, A. G., Jr., J. M. Soderblom, M. A. Donelan, J. W. Barnes and R. D. Lorenz (2016). Modeling and Observing the Role of Wind-Waves in Titan's Hydrocarbon Seas**:** P33F-06.
- Heavens, N. G., M. I. Richardson and A. D. Toigo (2008). "Two aerodynamic roughness maps derived from Mars Orbiter Laser Altimeter (MOLA) data and their effects on boundary layer properties in a Mars general circulation model (GCM)." Journal of Geophysical Research: Planets **113**(E2).
- Hébrard, E., C. Listowski, P. Coll, B. Marticorena, G. Bergametti, A. Määttänen, F. Montmessin and F. Forget (2012). "An aerodynamic roughness length map derived from extended Martian rock abundance data." Journal of Geophysical Research: Planets **117**(E4).
- Hofgartner, J. D., A. G. Hayes, J. I. Lunine, H. Zebker, R. D. Lorenz, M. J. Malaska, M. Mastrogiuseppe, C. Notarnicola and J. M. Soderblom (2016). "Titan's "Magic Islands": Transient features in a hydrocarbon sea." Icarus **271**: 338-349.
- Janssen, M. A., A. Le Gall, R. M. Lopes, R. D. Lorenz, M. J. Malaska, A. G. Hayes, C. D. Neish, A. Solomonidou, K. L. Mitchell, J. Radebaugh, S. J. Keihm, M. Choukroun, C. Leyrat, P. J. Encrenaz and M. Mastrogiuseppe (2016). "Titan's surface at 2.18-cm wavelength imaged by the Cassini RADAR radiometer: Results and interpretations through the first ten years of observation." Icarus **270**: 443-459.

References

- Jennings, D., V. Cottini, C. Nixon, R. Achterberg, F. Flasar, V. Kunde, P. Romani, R. Samuelson, A. Mamoutkine and N. Gorius (2016). "Surface temperatures on Titan during northern winter and spring." The Astrophysical Journal Letters **816**(1): L17.
- Jennings, D., F. Flasar, V. Kunde, R. Samuelson, J. Pearl, C. Nixon, R. Carlson, A. Mamoutkine, J. Brasunas and E. Guandique (2009). "Titan's surface brightness temperatures." The Astrophysical Journal Letters **691**(2): L103.
- Jennings, D. E., T. Tokano, V. Cottini, C. A. Nixon, R. K. Achterberg, F. M. Flasar, V. G. Kunde, P. N. Romani, R. E. Samuelson, M. E. Segura, N. J. P. Gorius, E. Guandique, M. S. Kaelberer and A. Coustenis (2019). "Titan Surface Temperatures during the Cassini Mission." The Astrophysical Journal **877**(1): L8.
- Khare, B. N., C. Sagan, E. T. Arakawa, F. Suits, T. A. Callcott and M. W. Williams (1984). "Optical constants of organic tholins produced in a simulated Titanian atmosphere: From soft x-ray to microwave frequencies." Icarus **60**(1): 127-137.
- Lancaster, N. (2004). "Relations between aerodynamic and surface roughness in a hyper-arid cold desert: McMurdo Dry Valleys, Antarctica." Earth Surface Processes and Landforms **29**(7): 853-867.
- Lee, X. (2018). Fundamentals of boundary-layer meteorology, Springer.
- Lopes, R., S. Wall, C. Elachi, S. P. Birch, P. Corlies, A. Coustenis, A. Hayes, J. Hofgartner, M. A. Janssen and R. Kirk (2019). "Titan as revealed by the Cassini radar." Space Science Reviews **215**(4): 33.
- Lopes, R. M., M. J. Malaska, A. M. Schoenfeld, A. Solomonidou, S. Birch, M. Florence, A. Hayes, D. Williams, J. Radebaugh and T. Verlander (2019). "A global geomorphologic map of Saturn's moon Titan." Nature Astronomy: 1-6.
- Lopes, R. M. C., S. D. Wall, C. Elachi, S. P. D. Birch, P. Corlies, A. Coustenis, A. G. Hayes, J. D. Hofgartner, M. A. Janssen, R. L. Kirk, A. LeGall, R. D. Lorenz, J. I. Lunine, M. J. Malaska, M. Mastroguiseppe, G. Mitri, C. D. Neish, C. Notarnicola, F. Paganelli, P. Paillou, V. Poggiali, J. Radebaugh, S. Rodriguez, A. Schoenfeld, J. M. Soderblom, A. Solomonidou, E. R. Stofan, B. W. Stiles, F. Tosi, E. P. Turtle, R. D. West, C. A. Wood, H. A. Zebker, J. W. Barnes, D. Casarano, P. Encrenaz, T. Farr, C. Grima, D. Hemingway, O. Karatekin, A. Lucas, K. L. Mitchell, G. Ori, R. Orosei, P. Ries, D. Riccio, L. A. Soderblom and Z. Zhang (2019). "Titan as Revealed by the Cassini Radar." Space Science Reviews **215**(4): 33.
- Lora, J. M., J. I. Lunine and J. L. Russell (2015). "GCM simulations of Titan's middle and lower atmosphere and comparison to observations." Icarus **250**: 516-528.
- Lora, J. M., J. I. Lunine, J. L. Russell and A. G. Hayes (2014). "Simulations of Titan's paleoclimate." Icarus **243**: 264-273.
- Lora, J. M. and J. L. Mitchell (2015). "Titan's asymmetric lake distribution mediated by methane transport due to atmospheric eddies." Geophysical Research Letters **42**(15): 6213-6220.
- Lora, J. M., T. Tokano, J. V. d'Ollone, S. Lebonnois and R. D. Lorenz (2019). "A model intercomparison of Titan's climate and low-latitude environment." Icarus **333**: 113-126.
- Lorenz, R. D., K. L. Mitchell, R. L. Kirk, A. G. Hayes, O. Aharonson, H. A. Zebker, P. Paillou, J. Radebaugh, J. I. Lunine, M. A. Janssen, S. D. Wall, R. M. Lopes, B. Stiles, S. Ostro, G. Mitri and E. R. Stofan (2008). "Titan's inventory of organic surface materials." Geophysical Research Letters **35**(2).
- MacKenzie, S. M., J. M. Lora and R. D. Lorenz (2019). "A thermal inertia map of Titan." Journal of Geophysical Research: Planets **124**(7): 1728-1742.
- Malaska, M. J., R. M. Lopes, D. A. Williams, C. D. Neish, A. Solomonidou, J. M. Soderblom, A. M. Schoenfeld, S. P.

References

Birch, A. G. Hayes and A. Le Gall (2016). "Geomorphological map of the Afekan Crater region, Titan: Terrain relationships in the equatorial and mid-latitude regions." Icarus **270**: 130-161.

- Malaska, M. J., R. M. C. Lopes, D. A. Williams, C. D. Neish, A. Solomonidou, J. M. Soderblom, A. M. Schoenfeld, S. P. D. Birch, A. G. Hayes, A. Le Gall, M. A. Janssen, T. G. Farr, R. D. Lorenz, J. Radebaugh and E. P. Turtle (2016). "Geomorphological map of the Afekan Crater region, Titan: Terrain relationships in the equatorial and mid-latitude regions." Icarus **270**: 130-161.
- Mastrapa, R., S. Sandford, T. Roush, D. Cruikshank and C. Dalle Ore (2009). "Optical constants of amorphous and crystalline H2O-ice: 2.5-22 μm (4000-455 cm–1) optical constants of H2O-ice." The Astrophysical Journal **701**(2): 1347.
- Mastrapa, R. M., M. P. Bernstein, S. A. Sandford, T. L. Roush, D. P. Cruikshank and C. M. D. Ore (2008). "Optical constants of amorphous and crystalline H2O-ice in the near infrared from 1.1 to 2.6 μm." Icarus **197**(1): 307-320.
- Mastrogiuseppe, M., V. Poggiali, A. G. Hayes, J. I. Lunine, R. Seu, G. Di Achille and R. D. Lorenz (2018). "Cassini radar observation of Punga Mare and environs: Bathymetry and composition." Earth and Planetary Science Letters **496**: 89-95.
- McKay, C. P., J. B. Pollack and R. Courtin (1989). "The thermal structure of Titan's atmosphere." Icarus **80**(1): 23-53.
- Meftah, M., L. Damé, D. Bolsée, A. Hauchecorne, N. Pereira, D. Sluse, G. Cessateur, A. Irbah, J. Bureau, M. Weber, K. Bramstedt, T. Hilbig, R. Thiéblemont, M. Marchand, F. Lefèvre, A. Sarkissian and S. Bekki (2018). "SOLAR-ISS: A new reference spectrum based on SOLAR/SOLSPEC observations★." A&A **611**: A1.
- Neish, C. D., R. D. Lorenz, R. L. Kirk and L. C. Wye (2010). "Radarclinometry of the sand seas of Africa's Namibia and Saturn's moon Titan." Icarus **208**(1): 385-394.
- Newman, C., M. Richardson and Y. Lian (2013). Investigating Titan's Surface-Atmosphere Interactions with a General Circulation Model. European Planetary Science Congress.
- Newman, C. E., M. I. Richardson, Y. Lian and C. Lee (2016). "Simulating Titan's methane cycle with the TitanWRF general circulation model." Icarus **267**: 106-134.
- Paganelli, F., M. A. Janssen, B. Stiles, R. West, R. D. Lorenz, J. I. Lunine, S. D. Wall, P. Callahan, R. Lopes and E. Stofan (2007). "Titan's surface from Cassini RADAR SAR and high resolution radiometry data of the first five flybys." Icarus **191**(1): 211-222.
- Poggiali, V., A. G. Hayes, M. Mastrogiuseppe, A. Le Gall, D. Lalich, I. Gómez-Leal and J. I. Lunine (2020). "The Bathymetry of Moray Sinus at Titan's Kraken Mare." Journal of Geophysical Research: Planets **125**(12): e2020JE006558.
- Pollack, J. B. (1973). "Greenhouse models of the atmosphere of titan." Icarus **19**(1): 43-58.
- Porco, C. C., E. Baker, J. Barbara, K. Beurle, A. Brahic, J. A. Burns, S. Charnoz, N. Cooper, D. D. Dawson, A. D. Del Genio, T. Denk, L. Dones, U. Dyudina, M. W. Evans, S. Fussner, B. Giese, K. Grazier, P. Helfenstein, A. P. Ingersoll, R. A. Jacobson, T. V. Johnson, A. McEwen, C. D. Murray, G. Neukum, W. M. Owen, J. Perry, T. Roatsch, J. Spitale, S. Squyres, P. Thomas, M. Tiscareno, E. P. Turtle, A. R. Vasavada, J. Veverka, R. Wagner and R. West (2005). "Imaging of Titan from the Cassini spacecraft." Nature **434**(7030): 159-168.
- Prigent, C., I. Tegen, F. Aires, B. Marticorena and M. Zribi (2005). "Estimation of the aerodynamic roughness length in arid and semi-arid regions over the globe with the ERS scatterometer." Journal of Geophysical

Research: Atmospheres **110**(D9).

- Reijmer, C., E. Van Meijgaard and M. Van den Broeke (2004). "Numerical studies with a regional atmospheric climate model based on changes in the roughness length for momentum and heat over Antarctica." Boundary-layer meteorology **111**(2): 313-337.
- Richardson, M. I. and R. J. Wilson (2002). "A topographically forced asymmetry in the Martian circulation and climate." Nature **416**(6878): 298-301.
- Smith, P., M. Lemmon, R. Lorenz, L. Sromovsky, J. Caldwell and M. Allison (1996). "Titan's surface, revealed by HST imaging." Icarus **119**(2): 336-349.
- Solomonidou, A., A. Coustenis, R. M. Lopes, M. J. Malaska, S. Rodriguez, P. Drossart, C. Elachi, B. Schmitt, S. Philippe and M. Janssen (2018). "The spectral nature of Titan's major geomorphological units: constraints on surface composition." Journal of Geophysical Research: Planets **123**(2): 489-507.
- Solomonidou, A., M. Hirtzig, A. Coustenis, E. Bratsolis, S. Le Mouélic, S. Rodriguez, K. Stephan, P. Drossart, C. Sotin, R. Jaumann, R. H. Brown, K. Kyriakopoulos, R. M. C. Lopes, G. Bampasidis, K. Stamatelopoulou-Seymour and X. Moussas (2014). "Surface albedo spectral properties of geologically interesting areas on Titan." Journal of Geophysical Research: Planets **119**(8): 1729-1747.
- Solomonidou, A., A. Le Gall, M. J. Malaska, S. P. D. Birch, R. M. C. Lopes, A. Coustenis, S. Rodriguez, S. D. Wall, R. J. Michaelides, M. R. Nasr, C. Elachi, A. G. Hayes, J. M. Soderblom, A. M. Schoenfeld, C. Matsoukas, P. Drossart, M. A. Janssen, K. J. Lawrence, O. Witasse, J. Yates and J. Radebaugh (2020). "Spectral and emissivity analysis of the raised ramparts around Titan's northern lakes." Icarus **344**: 113338.
- Takahashi, Y. O., H. Fujiwara, H. Fukunishi, M. Odaka, Y. Y. Hayashi and S. Watanabe (2003). "Topographically induced north-south asymmetry of the meridional circulation in the Martian atmosphere." Journal of Geophysical Research: Planets **108**(E3).
- Takahashi, Y. O., H. Fujiwara, H. Fukunishi, M. Odaka, Y. Y. Hayashi and S. Watanabe (2003). "Topographically induced north-south asymmetry of the meridional circulation in the Martian atmosphere." Journal of Geophysical Research: Planets **108**(E3).
- Taylor, P. A., R. I. Sykes and P. J. Mason (1989). "On the parameterization of drag over small-scale topography in neutrally-stratified boundary-layer flow." Boundary-Layer Meteorology **48**(4): 409-422.
- Tokano, T. (2005). "Meteorological assessment of the surface temperatures on Titan: constraints on the surface type." Icarus **173**(1): 222-242.
- Tokano, T. (2009). "Impact of seas/lakes on polar meteorology of Titan: Simulation by a coupled GCM-Sea model." Icarus **204**(2): 619-636.
- Tokano, T. (2019). "Orbitally and geographically caused seasonal asymmetry in Titan's tropospheric climate and its implication for the lake distribution." Icarus **317**: 337-353.
- Tokano, T., F. Ferri, G. Colombatti, T. Mäkinen and M. Fulchignoni (2006). "Titan's planetary boundary layer structure at the Huygens landing site." Journal of Geophysical Research: Planets **111**(E8).
- Tokano, T., C. P. McKay, F. M. Neubauer, S. K. Atreya, F. Ferri, M. Fulchignoni and H. B. Niemann (2006). "Methane drizzle on Titan." Nature **442**(7101): 432-435.
- Tokano, T. and F. M. Neubauer (2005). "Wind-induced seasonal angular momentum exchange at Titan's surface and its influence on Titan's length-of-day." Geophysical Research Letters **32**(24).
- Tokano, T., F. M. Neubauer, M. Laube and C. P. McKay (2001). "Three-Dimensional Modeling of the Tropospheric

Methane Cycle on Titan." Icarus **153**(1): 130-147.

- Turtle, E. P., J. E. Perry, J. M. Barbara, A. D. Del Genio, S. Rodriguez, S. Le Mouélic, C. Sotin, J. M. Lora, S. Faulk, P. Corlies, J. Kelland, S. M. MacKenzie, R. A. West, A. S. McEwen, J. I. Lunine, J. Pitesky, T. L. Ray and M. Roy (2018). "Titan's Meteorology Over the Cassini Mission: Evidence for Extensive Subsurface Methane Reservoirs." Geophysical Research Letters **45**(11): 5320-5328.
- Warren, S. G. and R. E. Brandt (2008). "Optical constants of ice from the ultraviolet to the microwave: A revised compilation." Journal of Geophysical Research: Atmospheres **113**(D14).
- Westley, M. S., G. A. Baratta and R. A. Baragiola (1998). "Density and index of refraction of water ice films vapor deposited at low temperatures." The Journal of Chemical Physics **108**(8): 3321-3326.
- Wiernga, J. (1993). "Representative roughness parameters for homogeneous terrain." Boundary-Layer Meteorology **63**(4): 323-363.
- Yusup, Y. (2012). "Aerodynamic drag coefficient over equatorial coastal industrialized and urban areas." Journal of Wind Engineering and Industrial Aerodynamics **110**: 25-39.